iScience

CellPress
OPEN ACCESS

Article

O^6-methylguanine DNA methyltransferase regulates β-glucan-induced trained immunity of macrophages via farnesoid X receptor and AMPK

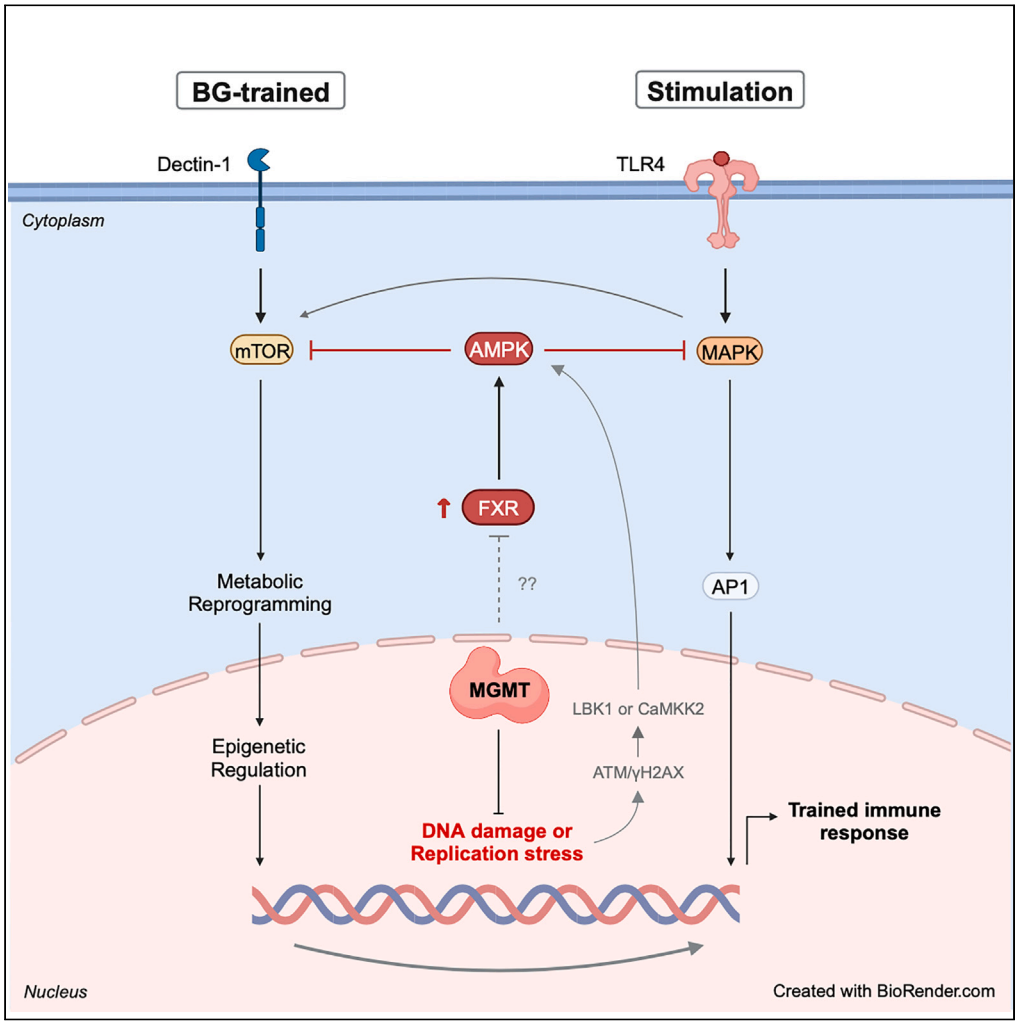

Salisa Benjaskulluecha, Atsadang Boonmee, MdFazlul Haque, ..., Benjawan Saechue, Patipark Kueanjinda, Tanapat Palaga

tanapat.p@chula.ac.th

Highlights

O^6-methylguanine DNA methyltransferase regulates β-glucan-induced trained immunity

MGMT deletion in macrophages reduced trained responses both *in vitro* and *in vivo*

MGMT regulates trained immunity via FXR/AMPK and mTOR/HIF1α pathways

Benjaskulluecha et al., iScience *27*, 108733
January 19, 2024
https://doi.org/10.1016/j.isci.2023.108733

iScience

CellPress
OPEN ACCESS

Article

O^6-methylguanine DNA methyltransferase regulates β-glucan-induced trained immunity of macrophages via farnesoid X receptor and AMPK

Salisa Benjaskulluecha,[1,2,3] Atsadang Boonmee,[2,3,4] MdFazlul Haque,[2,3] Benjawan Wongprom,[2,3] Thitiporn Pattarakankul,[3,5] Chitsuda Pongma,[3,6] Kittitach Sri-ngern-ngam,[2,3] Pornlapat Keawvilai,[3,6] Thadaphong Sukdee,[1,2,3] Benjawan Saechue,[2,3,7] Patipark Kueanjinda,[1,2,8] and Tanapat Palaga[1,2,3,9,*]

SUMMARY

Trained immunity is the heightened state of innate immune memory that enhances immune response resulting in nonspecific protection. Epigenetic changes and metabolic reprogramming are critical steps that regulate trained immunity. In this study, we reported the involvement of O^6-methylguanine DNA methyltransferase (MGMT), a DNA repair enzyme of lesion induced by alkylating agents, in regulation the trained immunity induced by β-glucan (BG). Pharmacological inhibition or silencing of MGMT expression altered LPS stimulated pro-inflammatory cytokine productions in BG-trained bone marrow derived macrophages (BMMs). Targeted deletion of *Mgmt* in BMMs resulted in reduction of the trained responses both *in vitro* and *in vivo* models. The transcriptomic analysis revealed that the dampening trained immunity in MGMT KO BMMs is partially mediated by ATM/FXR/AMPK axis affecting the MAPK/mTOR/HIF1α pathways and the reduction in glycolysis function. Taken together, a failure to resolve a DNA damage may have consequences for innate immune memory.

INTRODUCTION

Trained immunity describes an innate immune memory that enhance immune response during the second exposure to the pathogens.[1,2] In an *in vitro* system, trained immunity can be generated by priming of innate immune cells with specific pathogen-associated molecular patterns (PAMPs) or damage-associated molecular patterns (DAMPs) such as β-glucan (BG), Bacillus Calmette Guerin (BCG) vaccine and other metabolites such as oxidized low-density lipoprotein (oxLDL), and mevalonate.[1,3,4] These stimuli induce cells to poise for secondary stimulation, leading to heightened immune response to non-specific secondary stimulation. Besides a broad protective role of trained immunity after vaccination, the maladaptive trained immunity has been associated with numerous immunopathology and hyperinflammatory diseases such as allergy, atherosclerosis, and Alzheimer's disease.[1,5,6] Previous studies documented that epigenetic regulations and metabolic reprogramming are key mechanisms in generating innate immune memory.[7,8] However, the understanding of the underlying mechanisms is far from complete. The mechanisms how trained immunity is tightly regulated, may provide a new therapeutic strategy to re-balance the immune responses, better vaccine design and alleviate the undesirable disease outcomes.

O^6-Methylguanine-DNA methyltransferase (MGMT) is a DNA damage repair enzyme that functions in removing a methyl group from methylated guanine as a result of alkylating agent-derived DNA adduct. This enzymatic reaction is used to prevent base transversion and double strand DNA breaks by base-pair mismatch during DNA replication.[9–11] The repairing process covalently transfer the methyl group to the active site of MGMT which irreversibly converts MGMT into an inactivated form and leads to its rapid degradation.[9–11] Up until now, most studies on MGMT mainly focus on carcinogenesis as loss of MGMT is linked to mutations and tumor formation in various types of cancers.[9–11] On the other hand, overexpression of MGMT in cancer cells can also promote the resistance to alkylating chemotherapy.[9–11] Thus, MGMT specific inhibitors have been combined with chemotherapy to increase sensitivity to the treatment.[9] Besides its role in carcinogenesis, *MGMT* promoter has been reported to be hypermethylated and the expression of the gene is repressed in chronic inflammatory disease. As a result, reduction in MGMT expression may accelerate the progression of inflammatory-related diseases.[12–15]

[1]Interdisciplinary Graduate Program in Medical Microbiology, Graduate School, Chulalongkorn University, Bangkok 10330, Thailand
[2]Center of Excellence in Immunology and Immune-Mediated Diseases, Chulalongkorn University, Bangkok 10330, Thailand
[3]Department of Microbiology, Faculty of Science, Chulalongkorn University, Bangkok 10330, Thailand
[4]Department of Microbiology, Faculty of Medicine Siriraj Hospital, Mahidol University, Bangkok 10700, Thailand
[5]Center of Excellence in Advanced Materials and Biointerfaces, Chulalongkorn University, Bangkok 10330, Thailand
[6]Graduate Program in Biotechnology, Faculty of Science, Chulalongkorn University, Bangkok 10330, Thailand
[7]One Health Research Unit, Faculty of Veterinary Science, Mahasarakham University, Mahasarakham 44000, Thailand
[8]Department of Microbiology, Faculty of Medicine, Chulalongkorn University, Bangkok 10330, Thailand
[9]Lead contact
*Correspondence: tanapat.p@chula.ac.th
https://doi.org/10.1016/j.isci.2023.108733

Previously, we performed a screening of inhibitor library of numerous epigenetic modifying enzymes to identify novel proteins that control trained immunity in BG-primed bone marrow derived macrophages (BMMs). Among many hits, we identified MGMT as a novel regulator of trained immunity.[16] Inhibition of MGMT prior to priming by BG enhances the effect of trained immunity as measured by increased IL-6 and TNFα production upon LPS stimulation. However, the underlying mechanisms of how MGMT regulates trained immunity and the trained immune response in the absence of MGMT are still unexplored.

In this study, we generated and characterized myeloid specific MGMT knockout mice (LysM-cre$^{cre/+}$; MGMT$^{fl/fl}$) to investigate the role(s) of MGMT in trained immunity and the underlying mechanisms and to confirm an *in vivo* impact of MGMT deficiency in myeloid cells. We found that depletion of MGMT expression reduced BG-trained immune responses both *in vitro* and *in vivo*. Using transcriptomic approach, changes in several signaling pathways, including FXR/ATM/AMPK, mTOR/HIF1α and MAPK pathway were observed during trained responses in the absence of MGMT. The results obtained here provide an undocumented role of MGMT in trained immune responses in macrophages which may provide a novel therapeutic strategy against cancer and immune mediated diseases.

RESULTS

Inhibition of MGMT decreases BG-trained responses in BMMs

We first established the trained macrophage models *in vitro* by priming BMMs with BG, followed by resting and LPS stimulation as shown in Figure 1A. The expression profiles of MGMT were examined at 24 h after BG-priming and LPS stimulation. Interestingly, the protein level of MGMT significantly increased after the priming step with BG but significantly decreased after 48 h of resting period and LPS stimulation (Figures 1B and 1C). The upregulation of MGMT during BG priming suggests the possible involvement of MGMT in regulation of trained immunity by BG. Next, the activity of MGMT was inhibited by treatment with MGMT inhibitor, lomeguatrib, for the entire experiment as indicated in Figure 1A (yellow line). This treatment resulted in decreased TNFα and IL-6 production in BG-trained BMMs in lomeguatrib-dose dependent manner (Figures 1D and 1E). The doses of lomeguatrib used in this study did not interfere with the cell viability (Figure 1F).

The effect of lomeguatrib when applied only during BG priming (Figure S1A) was tested. As shown in Figures S1B and S1C, lomeguatrib applied only during priming resulted in increased TNFα and IL-6 production upon LPS stimulation. Similarly, when the transient silencing of *Mgmt* was performed 48 h prior to BG treatment, significantly enhanced IL-6 productions were observed whereas slight increase in TNFα level was observed but the levels did not reach statistical significance (Figures S1D and S1F). This effect of lomeguatrib was in sharp contrast with the results obtained when the inhibitor was present the entire duration of the experiments. Together with the results that we previously reported that there was no effect on BG-trained response when lomeguatrib was added only during LPS restimulation after BG treatment and resting,[16] MGMT may function during both BG stimulation and during the resting where cells are poised to the second stimulation.

To gain an insight into the effect of lomeguatrib on MGMT expression dynamics, the expression profiles of MGMT after inhibitor treatment at different times were investigated. As shown in the Figure S1G, the expression of MGMT recovered following LPS stimulation when MGMT inhibitor was applied only during BG stimulation while its level was reduced to basal level when the inhibitor was present during the entire experiment (Figure S1G). Taken together, interfering with MGMT activities during BG-induced trained immunity altered the cytokine levels induced by LPS stimulation, indicating its important role in trained immunity.

Targeted deletion of *Mgmt* reduced BG-trained immunity in *in vitro* and *in vivo* models

To precisely evaluate the effect of MGMT in trained immunity, mice with myeloid specific deletion of MGMT (MGMT KO) (LysM-cre$^{cre/+}$; MGMT$^{fl/fl}$) were generated. MGMT KO mice were born with no obvious changes in the phenotype and appearance (Figures S2A and S2B). The depletion of MGMT was confirmed in MGMT KO BMMs, compared to the littermate control (Figure 2A). BMMs from these mice were evaluated for the expression of macrophage markers, F4/80 and CD11b. As shown in Figures S2C and S2D, similar phenotypes and cellular morphology of BMMs from the control or MGMT KO mice were observed. There was no obvious difference in the white blood cell profiles (white blood cells, lymphocytes, monocytes and neutrophils) between WT and MGMT KO mice at 8–10 weeks old (Figure S2E).

BMMs from MGMT deficient or littermate control mice were subjected to BG-trained and LPS stimulation as indicated in Figure 1A. The level of TNFα from BG-trained BMMs from MGMT KO mice was significantly lower than the control, while the level of IL-6 also showed slight decrease, but the difference did not reach statistical significance (Figures 2B and 2C). When the transcripts of *Tnf*, *Il1b* and *Il6* were measured, MGMT KO BMMs showed drastic and significant decrease in all cytokines (Figures S3A–S3C). Cell viability in unstimulated cells, LPS treated cells or BG followed by LPS stimulated cells did not show difference between WT and MGMT KO BMMs (Figure S3D).

Because MGMT targets O^6-methylguanine and removes the methyl group to prevent mutation and DNA damage, the loss of MGMT is expected to trigger or activate a DNA damage and repair response. Therefore, the levels of phosphorylation of an ATM kinase, a key enzyme in the DNA damage response, and γH2AX, a molecular marker of DNA damage and repair, were measured in BMMs from WT and MGMT KO mice during BG treatment and LPS stimulation. As shown in Figures 2D and 2E, BG treatment slightly increased γH2AX in BMMs, indicating that DNA breaks occur during BG stimulation. More importantly, MGMT KO BMMs showed higher level of phosphorylated ATM and γH2AX in all time points tested. These results strongly indicated that BG stimulation results in a DNA repair response and MGMT plays a crucial role in DNA repair during BG trained response.

To test whether reducing BG-trained response in the absence of MGMT was reproducible in an *in vivo* model, BG and LPS were administered as described in Figure 2F and the sera cytokines were measured. As shown in Figure 2G, reduction in the level of TNFα was observed only in BG-trained MGMT KO mice, but not in the untrained mice after LPS administration, compared to littermate control. In addition, reduction in the levels of IL-1α and IL-10 was evident in BG-trained MGMT KO mice. In contrast, increased IFN-γ was found in BG-trained MGMT KO

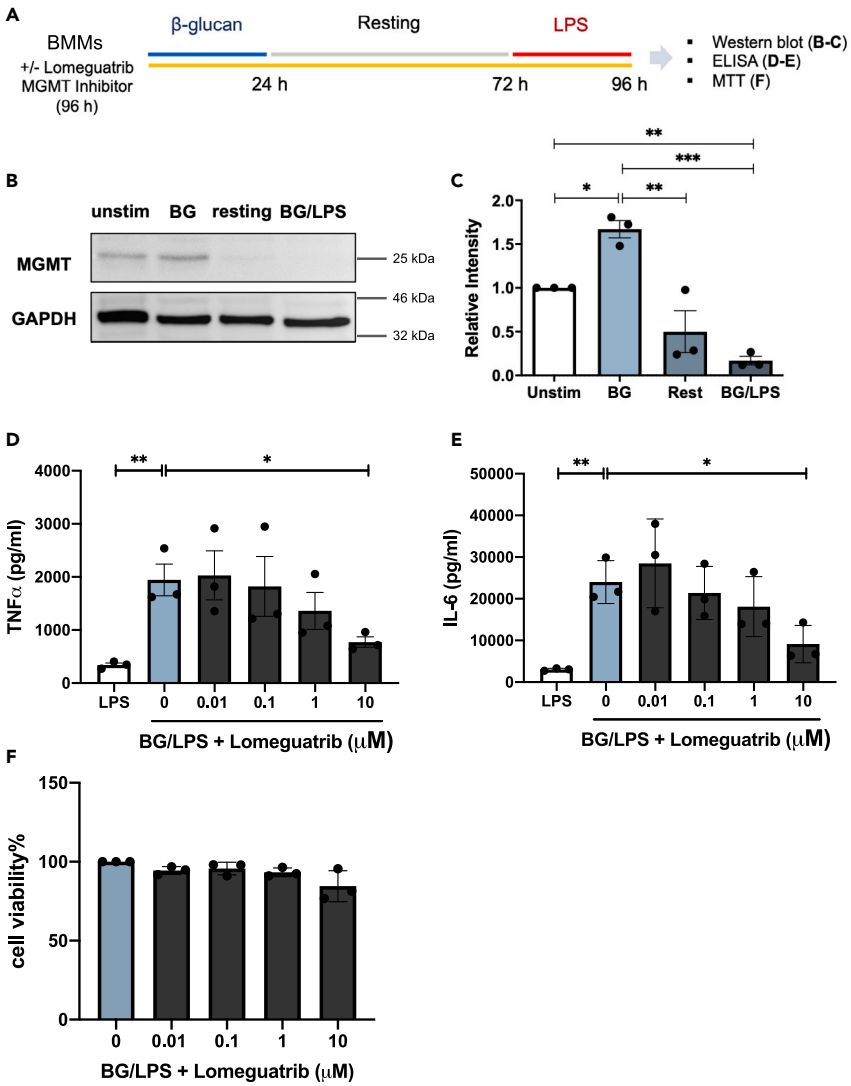

Figure 1. Effect of MGMT inhibition in BG-trained BMMs

(A) Protocol to induce BG-trained BMMs and the indicated time for inhibitor treatment (yellow line).

(B) Expression patterns of MGMT were detected by Western blot.

(C) The relative intensity of MGMT expression from Western blot was analyzed by ImageJ and normalized to GAPDH.

(D and E) The level of TNFα (D) and IL-6 (E) production in BG-trained BMMs after LPS stimulation that were treated with the different concentration of MGMT inhibitor lomeguatrib for 96 h.

(F) Cell viability from the MTT assay in BG-trained BMMs after treatment with different concentrations of lomeguatrib for 96 h. *, **, ***, and **** indicates significant difference compared by one-way ANOVA with Tukey's multiple test (C) and Dunnett's multiple test (B–D), compare the mean of each column with vehicle control BG/LPS (gray bar)) at $p < 0.05$, $p < 0.01$, $p < 0.001$ and $p < 0.0001$, respectively. (see also Figure S1).

mice (Figures 2H and S3E). Taken together, losing MGMT activity during BG-induced trained immunity severely compromised cytokine response in both *in vitro* and *in vivo* models.

BMMs from MGMT KO mice have altered transcriptomic profile

To further investigate how deficiency of MGMT alters the trained immunity in BMMs, we performed RNA sequencing of unstimulated (Unstim), BG-primed (BG24) and BG/LPS BMMs. As shown in Figure 3A, all transcriptomic data were clustered into three groups by PCA analysis based on the stimuli used with subtle difference between control and MGMT KO BMMs. The differentially expressed genes (DEGs) were compared and analyzed by DESeq2. To focus on the effect of MGMT KO in trained immunity, the expression profiles of DEGs in BG-primed and BG/LPS-stimulated WT vs. MGMT KO BMMs were normalized to the expression of unstimulated WT BMMs and represented as the

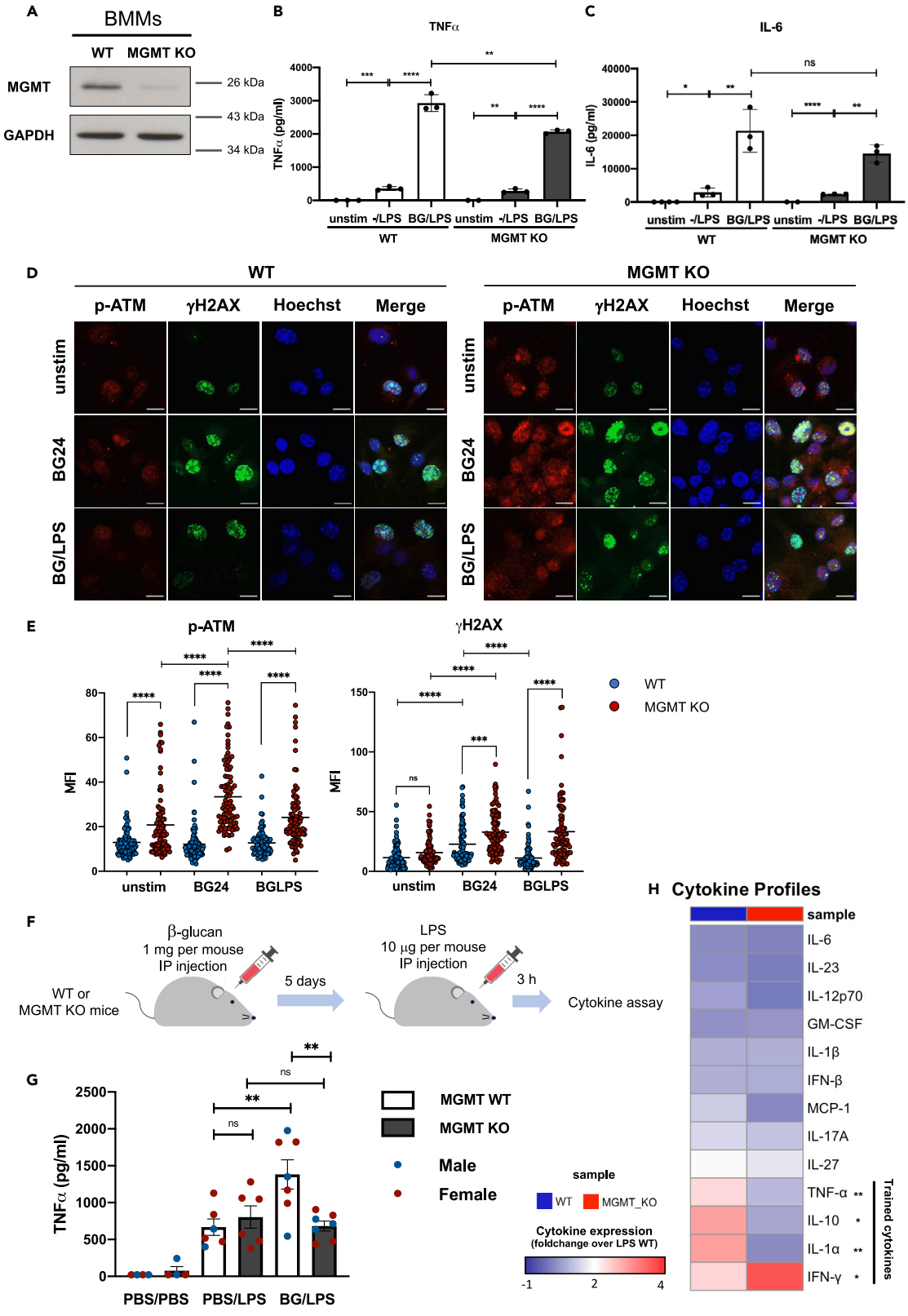
A
BMMs
WT MGMT KO
MGMT
GAPDH
26 kDa
43 kDa
34 kDa
B
TNFα
TNFα (pg/ml)
unstim -/LPS BG/LPS unstim -/LPS BG/LPS
WT
MGMT KO
C
IL-6
IL-6 (pg/ml)
unstim -/LPS BG/LPS unstim -/LPS BG/LPS
WT
MGMT KO
D
WT
MGMT KO
p-ATM γH2AX Hoechst Merge
unstim
BG24
BG/LPS
E
p-ATM
γH2AX
MFI
unstim BG24 BGLPS
WT
MGMT KO
F
β-glucan
1 mg per mouse
IP injection
WT or
MGMT KO mice
5 days
LPS
10 μg per mouse
IP injection
3 h
Cytokine assay
G
TNFα (pg/ml)
PBS/PBS PBS/LPS BG/LPS
MGMT WT
MGMT KO
Male
Female
H Cytokine Profiles
sample
IL-6
IL-23
IL-12p70
GM-CSF
IL-1β
IFN-β
MCP-1
IL-17A
IL-27
TNF-α
IL-10
IL-1α
IFN-γ
Trained cytokines
sample
WT MGMT_KO
Cytokine expression
(foldchange over LPS WT)
-1 2 4

Figure 2. Effect of *in vitro* and *in vivo* trained immunity in WT and MGMT KO mice

(A) MGMT expression profile in unstimulated WT and MGMT KO BMMs detected by Western blot.

(B and C) The level of TNFα (B) and IL-6 (C) production from unstimulated, LPS-stimulated or BG-primed in WT and MGMT KO BMMs was detected by ELISA at 24 h after LPS stimulation.

(D and E) Immunofluorescence staining of DNA repair enzyme ATM kinase (red), DNA damage marker γH2AX (green), nuclei (blue) in WT and MGMT KO BMMs after BG priming (BG24) and LPS stimulation (BG/LPS) (scale bar length = 10 μm). Mean fluorescence intensity (MFI) of each marker was analyzed by ImageJ.

(F) Protocol to induce *in vivo* trained immunity in WT (LysM-cre$^{+/+}$; MGMT$^{fl/fl}$, Littlemate control) and MGMT KO (LysM-cre$^{cre/+}$; MGMT$^{fl/fl}$) mice and indicated time point for blood collection.

(G) Level of serum TNFα was measured by multiplex ELISA at 3 h after LPS injection.

(H) Inflammatory cytokines production of in serum of trained mice was measured by multiplex ELISA at 3 h of LPS injection. *, **, ***, and **** indicate significant differences compared by two-tailed unpaired *t*-tests (B-C) and one-way ANOVA with Tukey's multiple test (D-E, G-H) at $p < 0.05$, $p < 0.01$, $p < 0.001$ and $p < 0.0001$, respectively. ns: not statistically significant (see also Figures S2 and S3).

heatmaps. As shown in Figure 3B, depletion of MGMT significantly induced specific DEGs profiles after the BG priming and LPS stimulation. Top 10 up/down regulated DEGs in each condition were shown in Figure 3C.

To further investigate how MGMT regulates trained immunity, DEGs of all conditions were compared and illustrated using a Venn diagram. The up/down DEGs in both BG-primed and BG/LPS-stimulated MGMT KO BMMs were listed in the Figure S4. The DEGs that were specifically expressed in each condition (red circles) were subjected to the Gene Set Enrichment Analysis (GSEA). As shown in Figures 3D and 3E, depletion of MGMT significantly increased the expression of genes involved in nuclear receptor metapathway, PI3K/AKT signaling, and malignant pleural mesothelioma. On the other hand, genes involved in MAPK signaling were significantly downregulated in BG-trained MGMT KO BMMs during LPS stimulation. To further confirm whether DNA damage and repair mechanism is involved in trained immunity, we filtered genes that are related to DNA damage and repair from DEGs list in MGMT KO BMMs (BG24 and BG/LPS). As expected, several up-regulated DEGs in MGMT KO BMMs are associated with a DNA damage and repair mechanism (Figure 3F and Table S1). These global changes in the transcriptomic profiles confirmed that MGMT KO increased DNA breaks and DNA damage and repair response during trained immune response in macrophages.

Targeted deletion of *Mgmt* altered downstream signaling cascades of TLR4 and Dectin-1 in BG-trained BMMs

From GSEA analysis, MAPK signaling pathway was downregulated in BG-trained MGMT KO BMMs. We therefore hypothesized that depletion of MGMT may interfere with this pathway downstream of TLR4. To test this hypothesis, activation of NF-κB and MAPK pathways were investigated in BG-trained BMMs after LPS stimulation. As shown in Figures 4A–4F, LPS stimulation significantly activated NF-κB and MAPK signaling pathways, including ERK, p38, and SAPK/JNK, in a time-dependent manner. When compared to WT BMMs, the level of phosphorylated p38, and SAPK/JNK, was significantly lower in the trained MGMT KO BMMs (Figures 4B, 4D, and 4F). Depletion of MGMT slightly decreased NF-κB and ERK activation, but the levels did not reach statistical significance (Figures 4B, 4C, and 4E). This result strongly indicates that depletion of MGMT interferes with TLR4 signaling in BG-trained BMMs without altering the levels of TLR4 on the cell surface (Figure S5A).

We next investigated whether the downstream signaling of Dectin-1, a surface receptor for BG, would be also affected in the MGMT KO BMMs. To answer this question, activation of AKT and mTOR/HIF1α pathway,[17,18] downstream signaling pathway of Dectin-1, was investigated in BG-trained MGMT KO BMMs. Activation of AKT pathway was detected by the phosphorylation of AKT at Thr308. As shown in Figure S5B, phosphorylation of AKT were clearly induced in WT and MGMT KO BMMs at 4 h after BG priming at a similar level. However, the activation of mTOR was significantly decreased in the MGMT KO BMMs (Figure 4G) while the expression of HIF1α reduced slightly but did not reach statistical significance (Figure 4H). Taken together, this result reveals the possible role of MGMT in regulation of downstream signaling molecules of Dectin-1 and TLR4 receptors.

Targeted deletion of *Mgmt* activated FXR/AMPK signaling and altered metabolic flux in BG-trained BMMs

As mTOR/HIF1α pathway directly regulate glycolysis function that is crucial for trained immune response, we performed a glycolysis stress assay which detect the level of glycolysis as an extracellular acidification rate (ECAR) by Seahorse XFp Analyzer. In this experiment, the glycolytic functions were investigated in unstimulated and BG-primed BMMs after resting for 48 h. As shown in Figures 5A–5E, depletion of MGMT decreased ECAR level in the BG-primed BMMs, but not in the unstimulated cells. The reduction of ECAR resulted in a decrease in both non-glycolytic acidification and glycolytic function, including glycolysis, glycolytic capacity, and glycolytic reserve in the BG-primed MGMT KO BMMs.

Next, we focused on the role of adenosine monophosphate-activated protein kinase (AMPK) which is a cellular energy sensor that acts as main regulator of MAPK and mTOR/HIF1α signaling pathway and glycolysis and inflammation.[19–21] As expected, the phosphorylation of AMPK was clearly induced at higher level in MGMT KO BG-trained BMMs after LPS stimulation (Figure 5F).

Among several DNA damage and repair DEGs in Figure 3F, we next focused on the farnesoid X receptor (FXR; encoded by *Nr1h4*) as the possible cellular switch that can regulate inflammatory process, AMPK signaling, glycolysis and DNA repair mechanism.[22–27] Based on our transcriptome data, FXR expression was significantly increased in MGMT KO BMMs after BG priming (Figures 3C–3F). Inhibition of FXR by its inhibitor, ursodeoxycholic acid (UDCA), during the resting period after BG priming significantly rescued the dampened cytokine production in BG-trained MGMT KO BMMs in a dose-dependent manner (Figures 5G–5I). These results indicated that MGMT may regulate trained immunity via AMPK and FXR.

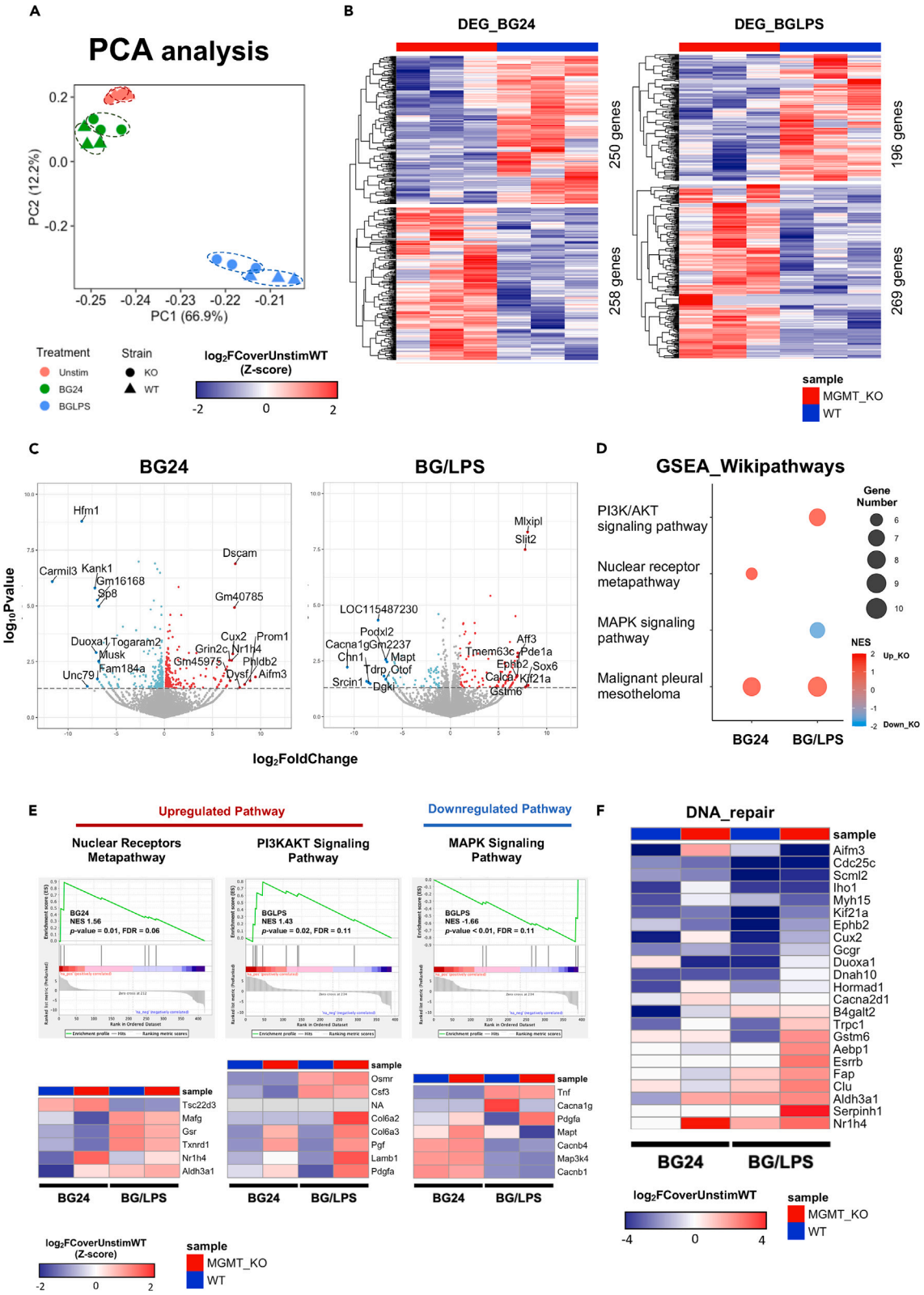
A
PCA analysis
PC2 (12.2%)
PC1 (66.9%)
Treatment
Unstim
BG24
BGLPS
Strain
KO
WT
log2FCoverUnstimWT (Z-score)
B
DEG_BG24
DEG_BGLPS
250 genes
258 genes
196 genes
269 genes
sample
MGMT_KO
WT
C
BG24
BG/LPS
log10Pvalue
log2FoldChange
D
GSEA_Wikipathways
PI3K/AKT signaling pathway
Nuclear receptor metapathway
MAPK signaling pathway
Malignant pleural mesotheloma
Gene Number
NES
Up_KO
Down_KO
E
Upregulated Pathway
Downregulated Pathway
Nuclear Receptors Metapathway
PI3KAKT Signaling Pathway
MAPK Signaling Pathway
F
DNA_repair

Figure 3. Transcriptomic profile of WT and MGMT KO BMMs

(A) PCA analysis of transcriptomic profile in unstimulated, BG24 and BGLPS WT and MGMT KO BMMs are shown.

(B) Heatmap of differentially expressed genes (DEGs) in MGMT KO BMMs after BG-priming (BG24) and LPS stimulation (BG/LPS) analyzed by DESeq2 (p value cut off <0.05).

(C) Volcano plots between $\log_{10}$p value and $\log_2$foldchange of each gene in BG24 and BGLPS are shown.

(D and E) GSEA analysis of specifically expressed DEGs in BG-primed and BG-trained MGMT KO BMMs (p value cut off <0.05, FDR cut off <0.25).

(F) Upregulated DEGs associated with DNA damage and repair mechanism in MGMT KO BMMs. (see also Figure S4 and Table S1).

DISCUSSION

Trained immunity is the enhanced phenotype of innate memory. After previous infections or vaccinations, it was shown that the changes in epigenetic modifications such as histone methylation and the shift in metabolic flux from oxidative phosphorylation to aerobic glycolysis are crucial for induction of the trained phenotype in myeloid cells.[2,28] We reported here that a DNA repair enzyme, MGMT, which functions during DNA damage caused by alkylating agents, also plays a role in regulating trained immunity.[11]

As the main biological function of MGMT is to remove the methyl DNA adducts of O^6-MG caused by alkylating agents, loss of MGMT function potentially leads to accumulation of the O^6-MG lesions and possible DNA double-strand breaks and mutations. Besides the exogenous alkylating agents, O^6-MG may arise as the results of the endogenous source such as S-adenosyl methionine (SAM) and endogenous N-nitroso compounds (NOC) from food.[10,29] Indeed, significantly increased pATM and γH2AX were detected in MGMT KO BMMs (Figures 2D and 2E), indicating increased accumulation of DNA damage lesions and replication stress during BG stimulation and LPS restimulation. Until now, only limited reports have linked DNA damage to innate trained immunity. Interestingly, it was found that trained immunity induced in hematopoietic stem cells and progenitor cells prevents LPS-induced DNA damage and allows the bone marrow to mount protective responses to a secondary LPS challenge.[6] Further experiments are required to investigate whether accumulation of the O^6-MG occurs during trained immunity induction and its endogenous causative agents are directly involved in trained immunity in BMMs.

In addition to its role in DNA repair and cancer, MGMT has been linked to inflammation, as hypermethylation of its promoter is associated with chronic inflammatory diseases and chronic infectious diseases.[12,14,15] Although global MGMT knockout mice are susceptible to the lethal effect of alkylating agents,[30] specific deletion of MGMT in myeloid cells did not affect the growth and the overall general phenotypes of the mice (Figure S2). Both *in vivo* and *in vitro* data obtained in our study revealed a specific role of MGMT in myeloid cells in the context of BG-trained immune responses. Because applying MGMT inhibitor only during LPS restimulation did not show any effect on cytokine production,[16] it is likely that MGMT mainly participates in regulating the trained immunity during BG treatment and/or resting period, possibly by repairing O^6-MG that is induced by BG treatment.

Interestingly, when inhibitor of MGMT or siRNA approaches were employed to transiently inhibit MGMT function during BG priming, the results were opposite from those obtained from MGMT KO BMM or the use of inhibitor the entire duration of the experiments (Figures 1D and 1E vs. Figure S1). These opposing results indicate that the role of MGMT in trained immunity depends on the specific time point and the duration of inhibition. When MGMT is inhibited only during BG treatment, its expression recovered during the resting and LPS restimulation as observed by Western blot (Figure S1G). In contrast, the expression of MGMT during the resting and LPS restimulation were at low level in the vehicle control treatment. It is well documented that MGMT is a suicidal enzyme, and it is targeted for degradation by proteasome degradation after its enzymatic function.[31] Therefore, MGMT inhibitor may lead to degradation of MGMT once it is bound by inhibitor that mimics its specific substrate as observed in Figure S1G. In addition, mTOR target NDRG1 binds and stabilizes MGMT in a tumor model.[32] The aberration in MGMT re-expression during the resting period and LPS restimulation after a transient inhibition may induce higher trained response. Thus, MGMT may play an active role in regulating response during the BG training period. In contrast, its downregulation during the resting and/or LPS restimulation may be required for optimal responses. Consistent with this hypothesis, lomeguatrib treatment only during LPS restimulation did not show any effect on cytokine production in BG-trained BMMs. A transcriptomic investigation of lomeguatrib treatment only during BG treatment warrants further investigation that will shed light on differential roles of MGMT in BG stimulation.

The reduction of some sera cytokines was also observed when MGMT KO mice were induced for trained immunity *in vivo*. However, IFN-γ was the only cytokine that shows higher level than the control (Figures 2H and S4E). Because macrophages produce relatively low level of IFN-γ, the increase in IFN-γ production may derive from other immune cells such as T helper type 1 or NK cells. It has been shown that induction of the trained immunity *in vivo* depends on other immune cells for optimal trained response.[33] In one study, an innate immune training by BG promotes an anti-tumor phenotype in neutrophils through epigenetic reprogramming of granulopoiesis.[34] In our LysM-cre mouse model, monocytes/macrophages and neutrophils are the targets for gene deletion.[35] The impact of MGMT on trained response of neutrophils requires further investigation.

From the transcriptomic analysis in MGMT KO BMMs, depletion of MGMT dampened numerous signaling pathways, including mTOR/HIF1α signaling in trained BMMs (Figures 4G and 4H). One of the master regulators that modulates mTOR/HIF1α pathway and glycolysis is AMPK which is a cellular energy sensor.[36,37] Activation of AMPK by metformin has been reported to inhibit the effect of trained immunity in BMMs.[18] Moreover, AMPK activation negatively regulates activation of signaling molecules of MAPK such as c-Jun N-terminal protein kinase (JNK) which lead to repress inflammation.[38–41] In this study, we found that activation of AMPK significantly increased in MGMT KO BMMs (Figure 5F). Consistent with the activation of AMPK, decreased mTOR and the aerobic glycolysis which is required for trained BMMs were observed (Figures 5A–5E).[18–21] Furthermore, decrease in glycolytic function may interfere with the deposition of specific epigenetic marks during trained immunity.[18,42]

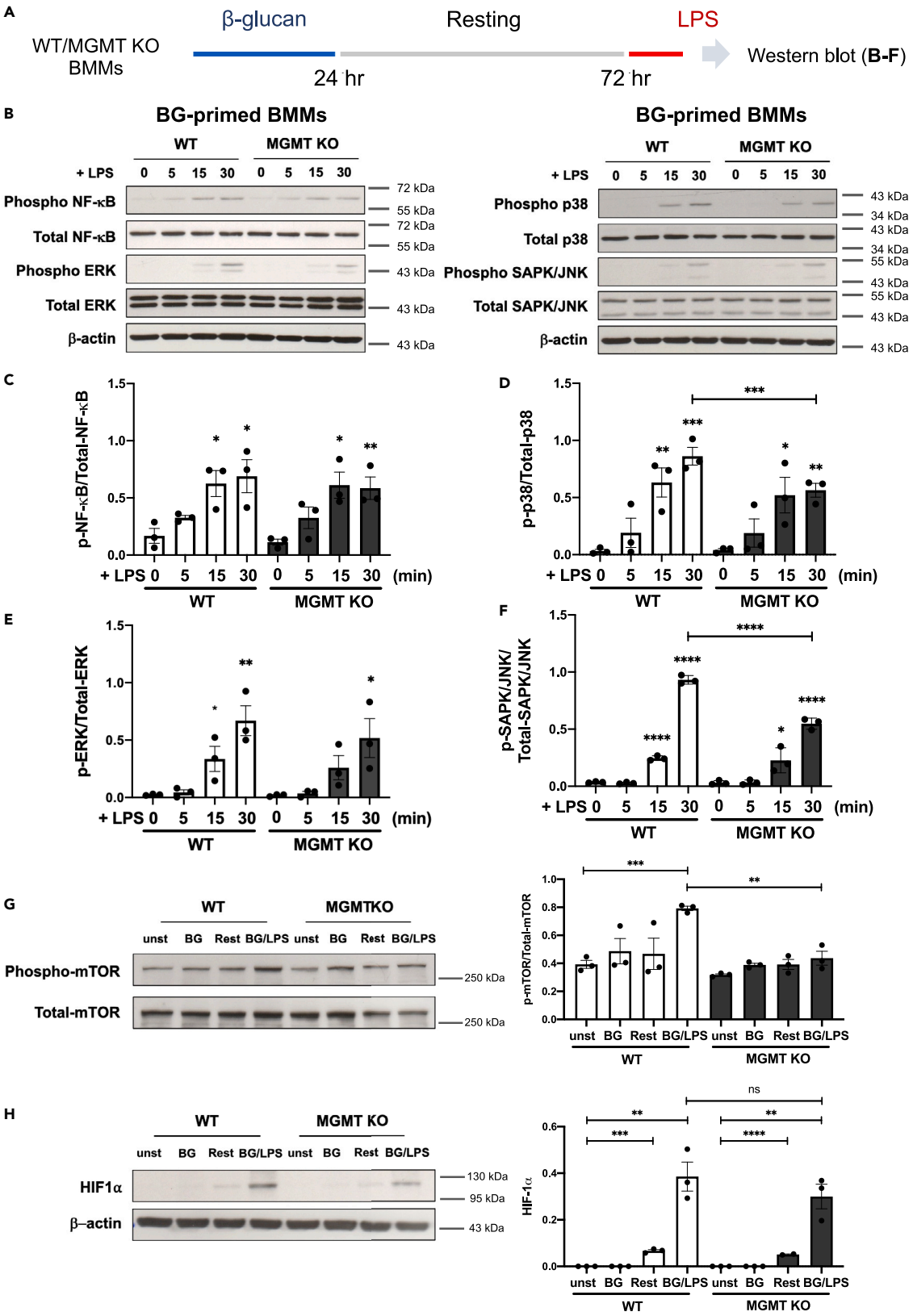
A
WT/MGMT KO BMMs
β-glucan
24 hr
Resting
72 hr
LPS
Western blot (B-F)
B
BG-primed BMMs
WT
MGMT KO
+ LPS 0 5 15 30 0 5 15 30
Phospho NF-κB
Total NF-κB
Phospho ERK
Total ERK
β-actin
72 kDa
55 kDa
43 kDa
BG-primed BMMs
Phospho p38
Total p38
Phospho SAPK/JNK
Total SAPK/JNK
34 kDa
C
p-NF-κB/Total-NF-κB
D
p-p38/Total-p38
E
p-ERK/Total-ERK
F
p-SAPK/JNK/ Total-SAPK/JNK
(min)
G
MGMTKO
unst BG Rest BG/LPS unst BG Rest BG/LPS
Phospho-mTOR
Total-mTOR
250 kDa
p-mTOR/Total-mTOR
H
HIF1α
β–actin
130 kDa
95 kDa
HIF-1α
ns

Figure 4. Downstream signaling profiles of TLR4 and Dectin-1 receptor in WT and MGMT KO BG-trained BMMs

(A) Experimental scheme and indicated time point for cell lysate collection for (B–F).

(B) NF-κB and MAPK signaling profiles in BG-trained WT and MGMT KO BMMs were detected by Western blot assay at indicated time point after LPS stimulation.

(C–F) Levels of phosphorylated NF-κB (C), p38 (D), ERK (E), and SAPK/JNK (F) were analyzed by ImageJ. The relative intensity was normalized to the total form of each protein.

(G and H) mTOR (G) and HIF1α (H) signaling profile in WT and MGMT KO BMMs was detected by Western blot assay after BG priming, resting and LPS stimulation. Relative intensity was analyzed by ImageJ. The intensities of phosphorylated mTOR and HIF1α were normalized to the total mTOR or β-actin. *, **, ***, and **** indicate significant differences compared by two-tailed unpaired *t*-tests at $p < 0.05$, $p < 0.01$, $p < 0.001$ and $p < 0.0001$, respectively. * over the bars represent statistical differences compared to the BG-primed WT or MGMT KO BMMs without LPS stimulation (LPS 0 min). (see also Figure S5).

In MGMT KO macrophages, increased phosphor-ATM and γH2AX were detected (Figures 2D and 2E), indicating increased DNA double-strand break. Similarly, increased AMPK activation was also detected in trained MGMT KO macrophages (Figure 5F). The DNA damage response can lead to PI3K/AKT activation[43] and increased PI3K/AKT pathway was enriched in MGMT KO macrophages (Figures 3D and 3E). In contrast, AMPK activation inhibits mTOR activation.[43–45] The balance between the two signaling pathways which dictates the activation status of mTOR pathway may influence the outcome of the trained immunity. Thus, it is possible that the mild effect of MGMT KO on trained immune response may be the result of these two opposing signaling pathways that determine the activation status of mTOR.

Among several DEGs that are associated with DNA damage and repair mechanism, nuclear receptor subfamily 1 group H member 4 (*Nr1h4*) encoding a farnesoid X receptor (FXR) was upregulated in BG-trained MGMT KO BMMs after BG priming (Figures 3C–3F). FXR is a bile acid receptor that negatively regulates several metabolic pathways such as lipid metabolism, gluconeogenesis, and glycolysis.[24,25,46,47] Moreover, activation of FXR also interferes with the downstream signaling of TLR4 by several mechanisms such as interfering with the binding of MAPK-AP1 transcription factor[48,49] and preventing the clearance of nuclear receptor corepressor 1 (NCoR1) complex[23,50,51] on the promoter of inflammatory genes during TLR4 activation. The use of FXR inhibitor, UDCA, restored the cytokine production in BG-trained MGMT KO BMMs (Figures 5G–5I). Thus, FXR may be one of the key links between MGMT and AMPK, as activation of FXR has been reported to promote the phosphorylation of AMPK.[22] Apart from the role in metabolic regulation, FXR functions are linked to DNA repair as it has a role to promote liver regeneration and repair after chemotherapeutic agents in several studies.[26,27] Besides FXR, ATM kinase, a DNA repair enzyme that increased in MGMT KO (Figures 2D and 2E), also promotes the activation of AMPK through its downstream signaling LBK1 and CaMKK2.[52–54] Further, activation of AMPK has been reported to be involved in several DNA repair processes.[54–58] Taken together, our results indicated that up-regulation FXR/ATM/AMPK axis may be responsible for promoting the DNA repair process and regulation of trained immunity in MGMT KO BMMs.

Because MGMT is not a transcription factor, it may regulate gene expression indirectly by interacting with other proteins. Based on the literature search, the possible MGMT-interacting proteins were metabolic enzyme pyruvate kinase and proteins related to epigenetic regulation such as SETs and several histone proteins are potential interacting proteins with MGMT.[59] This finding highlights the link between MGMT and epigenetic and metabolic regulations. Furthermore, the epigenetic regulator PR domain zinc figure protein 5 (*Prdm5*) was significantly increased in BG-trained MGMT KO BMMs. This protein can promote transcription repression by recruitment of G9a/GLP histone methyltransferase and HDAC1.[60,61]

Taken together, we propose a model where MGMT functions to repair O^6-MG during BG priming to prevent the activation of DNA damage pathway and activation of AMPK. In the absence of MGMT, AMPK is activated possibly through FXR and/or DNA repair response ATM. Activation of AMPK dampens mTOR signaling and alters metabolic flux resulting in decreased trained immune response. Thus, trained immunity may rely on a DNA repair mechanism in maintaining signaling pathways, metabolic flux and epigenetic modification for enhanced innate immune response.

Limitations of the study

In this study, we investigated the relevance of MGMT in BG-induced trained immunity in murine BMMs and in myeloid-specific MGMT deleted mice. It is not known whether trained immunity is also required MGMT for optimal trained response. In addition, as more stimuli can condition cells for trained immunity, including BCG, oxLDL, and heme, it is not known whether MGMT is also involved in the trained immune response induced by other stimuli besides BG. Lastly, in the mouse model where *Mgmt* is deleted in the myeloid lineage cells using the LysM-cre driver, neutrophils are also targeted in this system. The role of MGMT in neutrophils warrants further investigations.

STAR★METHODS

Detailed methods are provided in the online version of this paper and include the following:

- KEY RESOURCES TABLE
- RESOURCE AVAILABILITY
  - Lead contact
  - Materials availability
  - Data and code availability
- EXPERIMENTAL MODEL AND STUDY PARTICIPANT DETAILS
  - Construction of mouse model

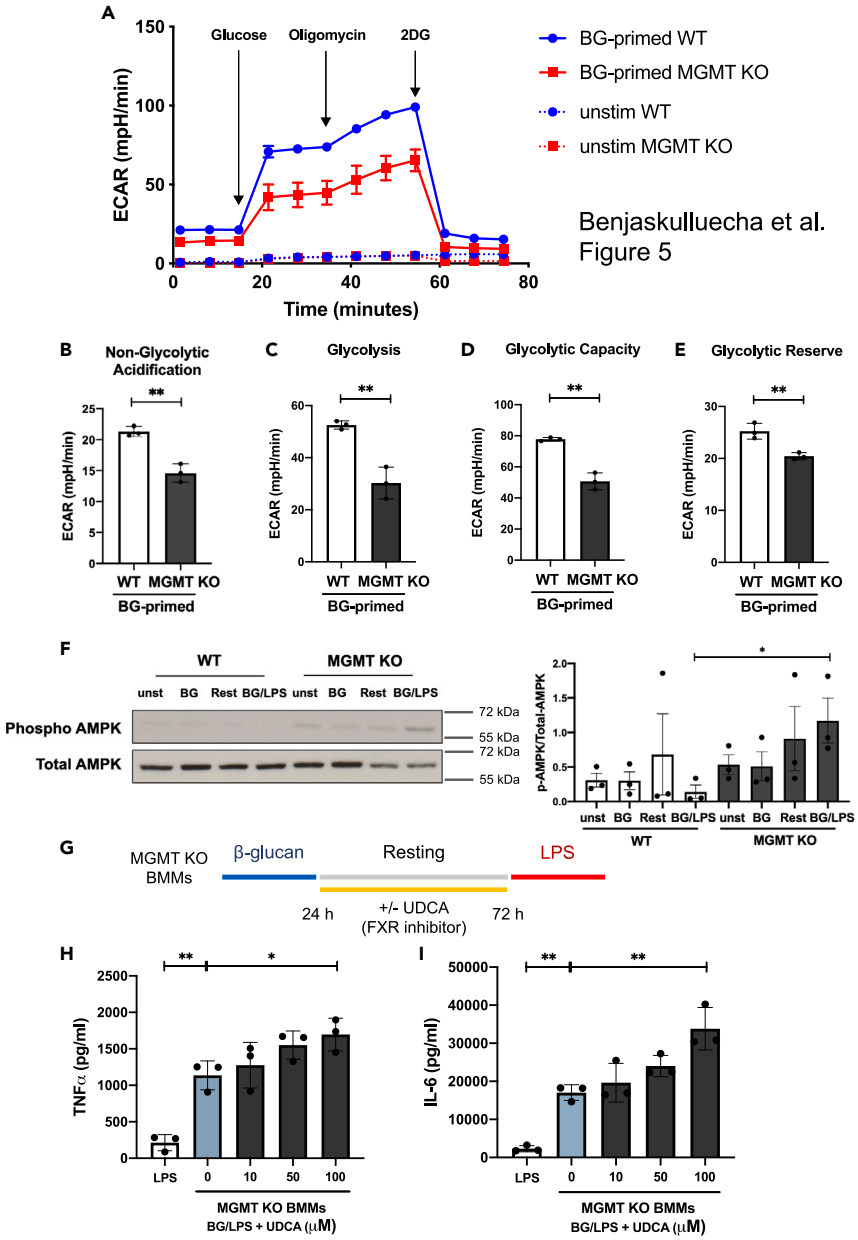

Figure 5. Metabolic and related signaling profiles of MGMT KO BMMs

(A) ECAR from glycolysis stress assay in unstimulated and BG-primed WT and MGMT KO BMMs after resting for 48 h (F) ECAR from of glycol-stress analysis in BG-trained BMMs: (B) non-glycolytic acidification, (C) normal glycolysis, (D) glycolytic capacity, and (E) glycolytic reserve.

(F) Phosphorylation of AMPK in WT and MGMT KO BG-trained BMMs was detected by Western blot assay after BG priming, resting and LPS stimulation. Relative intensity was analyzed by ImageJ. The intensities of phosphorylated AMPK were normalized to total AMPK.

(G) Indicate time for treatment of FXR inhibitor ursodeoxycholic acid (UDCA).

(H and I) The level of TNFα (H) and IL-6 (I) production in BG-trained MGMT KO BMMs that were treated with the different concentration of UDCA in resting period for 48 h (yellow line in G). *, **, ***, and **** indicate significant difference by two-tailed unpaired *t*-test at $p < 0.05$, $p < 0.01$, $p < 0.001$ and $p < 0.0001$, respectively.

- Isolation and culture of bone marrow derived macrophages (BMMs)
- METHOD DETAILS
  - Generation of BG-trained BMMs
  - siRNA mediated silencing of *Mgmt* expression
  - *In vivo* model for trained immunity
  - Complete blood count assay

- RNA sequencing and data analysis
- Western blot
- RT-qPCR
- MTT assay
- Immunofluorescence staining of DNA damage and DNA repair markers
- Glycolysis stress assay

- QUANTIFICATION AND STATISTICAL ANALYSIS

SUPPLEMENTAL INFORMATION

Supplemental information can be found online at https://doi.org/10.1016/j.isci.2023.108733.

ACKNOWLEDGMENTS

This research is funded by Thailand Science Research and Innovation Fund Chulalongkorn University (CU_FRB65_hea (62) _125_23_55), the NSRF via the Program Management Unit for Human Resources & Institutional Development, Research and Innovation (grant number B16F640117 and B16F640175) and the National Research Council of Thailand (811/2563). S.B. is supported by the scholarship from "The 100th Anniversary Chulalongkorn University Fund for Doctoral Scholarship" and "The 90th Anniversary Chulalongkorn University Fund (Ratchadaphiseksomphot Endowment Fund)" Chulalongkorn University. A.B. and F.H. are supported by the Second Century Fund (C2F), Chulalongkorn University. The study is also funded partly by Chulalongkorn University Laboratory Animal Center (CULAC) under protocol No. 2073016. We are grateful for the kind help with confocal microscope by Budsaraporn Boonsuth, Oral Biology Research Center, Faculty of Dentistry, Chulalongkorn university, Bangkok 10330, Thailand.

AUTHOR CONTRIBUTIONS

S.B. designed and performed all experiments, analyzed all data and prepared all figures and drafted the manuscripts. A.B., B.W., T.P.K., F.H., K.S., P.K.L., and T.S. performed ELISA, PCR, and Western blot and analyzed the data in some experiments. A.B., C.P., and B.S. performed *in vivo* experiments. P.K.D. prepared some figures. T.P.G. supervised the overall project, acquired grant funding, designed all experiments, analyzed data, and prepared the manuscript.

DECLARATION OF INTERESTS

The authors declare no conflict of interests.

INCLUSION AND DIVERSITY

We support inclusive, diverse, and equitable conduct of research.

Received: May 9, 2023
Revised: October 10, 2023
Accepted: December 11, 2023
Published: December 14, 2023

REFERENCES

1. Netea, M.G., Domínguez-Andrés, J., Barreiro, L.B., Chavakis, T., Divangahi, M., Fuchs, E., Joosten, L.A.B., van der Meer, J.W.M., Mhlanga, M.M., Mulder, W.J.M., et al. (2020). Defining trained immunity and its role in health and disease. Nat. Rev. Immunol. *20*, 375–388.
2. Al, B., Suen, T.K., Placek, K., and Netea, M.G. (2023). Innate (learned) memory. J. Allergy Clin. Immunol. *152*, 551–566.
3. Fanucchi, S., Dominguez-Andres, J., Joosten, L.A.B., Netea, M.G., and Mhlanga, M.M. (2020). The Intersection of Epigenetics and Metabolism in Trained Immunity. Immunity *54*, 32–43.
4. Domínguez-Andrés, J., Arts, R.J.W., Bekkering, S., Bahrar, H., Blok, B.A., de Bree, L.C.J., Bruno, M., Bulut, Ö., Debisarun, P.A., Dijkstra, H., et al. (2021). In vitro induction of trained immunity in adherent human monocytes. STAR Protoc. *2*, 100365.
5. Ochando, J., Mulder, W.J.M., Madsen, J.C., Netea, M.G., and Duivenvoorden, R. (2023). Trained immunity - basic concepts and contributions to immunopathology. Nat. Rev. Nephrol. *19*, 23–37.
6. Hajishengallis, G., Li, X., Mitroulis, I., and Chavakis, T. (2019). Trained Innate Immunity and Its Implications for Mucosal Immunity and Inflammation. Adv. Exp. Med. Biol. *1197*, 11–26.
7. Bekkering, S., Domínguez-Andrés, J., Joosten, L.A.B., Riksen, N.P., and Netea, M.G. (2021). Trained Immunity: Reprogramming Innate Immunity in Health and Disease. Annu. Rev. Immunol. *39*, 667–693.
8. Riksen, N.P., and Netea, M.G. (2021). Immunometabolic control of trained immunity. Mol. Aspects Med. *77*, 100897.
9. Gerson, S.L. (2004). MGMT: its role in cancer aetiology and cancer therapeutics. Nat. Rev. Cancer *4*, 296–307.
10. Fahrer, J., and Kaina, B. (2013). O6-methylguanine-DNA methyltransferase in the defense against N-nitroso compounds and colorectal cancer. Carcinogenesis *34*, 2435–2442.
11. Yu, W., Zhang, L., Wei, Q., and Shao, A. (2019). O(6)-Methylguanine-DNA Methyltransferase (MGMT): Challenges and New Opportunities in Glioma Chemotherapy. Front. Oncol. *9*, 1547.
12. Teuber-Hanselmann, S., Worm, K., Macha, N., and Junker, A. (2021). MGMT-Methylation in Non-Neoplastic Diseases of the Central Nervous System. Int. J. Mol. Sci. *22*, 3845.
13. Mokarram, P., Kavousipour, S., Sarabi, M.M., Mehrabani, G., Fahmidehkar, M.A., Shamsdin, S.A., Alipour, A., and Naini, M.A. (2015). MGMT-B gene promoter

hypermethylation in patients with inflammatory bowel disease - a novel finding. Asian Pac. J. Cancer Prev. *16*, 1945–1952.
14. Guzmán, L., Depix, M.S., Salinas, A.M., Roldán, R., Aguayo, F., Silva, A., and Vinet, R. (2012). Analysis of aberrant methylation on promoter sequences of tumor suppressor genes and total DNA in sputum samples: a promising tool for early detection of COPD and lung cancer in smokers. Diagn. Pathol. *7*, 87.
15. Su, P.F., Lee, T.C., Lin, P.J., Lee, P.H., Jeng, Y.M., Chen, C.H., Liang, J.D., Chiou, L.L., Huang, G.T., and Lee, H.S. (2007). Differential DNA methylation associated with hepatitis B virus infection in hepatocellular carcinoma. Int. J. Cancer *121*, 1257–1264.
16. Benjaskulluecha, S., Boonmee, A., Pattarakankul, T., Wongprom, B., Klomsing, J., and Palaga, T. (2022). Screening of compounds to identify novel epigenetic regulatory factors that affect innate immune memory in macrophages. Sci. Rep. *12*, 1912.
17. Bekkering, S., Arts, R.J.W., Novakovic, B., Kourtzelis, I., van der Heijden, C.D.C.C., Li, Y., Popa, C.D., Ter Horst, R., van Tuijl, J., Netea-Maier, R.T., et al. (2018). Metabolic Induction of Trained Immunity through the Mevalonate Pathway. Cell *172*, 135–146.e9.
18. Cheng, S.C., Quintin, J., Cramer, R.A., Shepardson, K.M., Saeed, S., Kumar, V., Giamarellos-Bourboulis, E.J., Martens, J.H.A., Rao, N.A., Aghajanirefah, A., et al. (2014). mTOR- and HIF-1alpha-mediated aerobic glycolysis as metabolic basis for trained immunity. Science *345*, 1250684.
19. Hu, M., Chen, X., Ma, L., Ma, Y., Li, Y., Song, H., Xu, J., Zhou, L., Li, X., Jiang, Y., et al. (2019). AMPK Inhibition Suppresses the Malignant Phenotype of Pancreatic Cancer Cells in Part by Attenuating Aerobic Glycolysis. J. Cancer *10*, 1870–1878.
20. Han, Y., He, M., Marin, T., Shen, H., Wang, W.T., Lee, T.Y., Hong, H.C., Jiang, Z.L., Garland, T., Jr., Shyy, J.Y.J., et al. (2021). Roles of KLF4 and AMPK in the inhibition of glycolysis by pulsatile shear stress in endothelial cells. Proc. Natl. Acad. Sci. USA *118*, e2103982118.
21. Sadria, M., and Layton, A.T. (2021). Interactions among mTORC, AMPK and SIRT: a computational model for cell energy balance and metabolism. Cell Commun. Signal. *19*, 57.
22. Lee, C.G., Koo, J.H., and Kim, S.G. (2015). Phytochemical regulation of Fyn and AMPK signaling circuitry. Arch Pharm. Res. (Seoul) *38*, 2093–2105.
23. Yao, J., Zhou, C.S., Ma, X., Fu, B.Q., Tao, L.S., Chen, M., and Xu, Y.P. (2014). FXR agonist GW4064 alleviates endotoxin-induced hepatic inflammation by repressing macrophage activation. World J. Gastroenterol. *20*, 14430–14441.
24. Trabelsi, M.S., Daoudi, M., Prawitt, J., Ducastel, S., Touche, V., Sayin, S.I., Perino, A., Brighton, C.A., Sebti, Y., Kluza, J., et al. (2015). Farnesoid X receptor inhibits glucagon-like peptide-1 production by enteroendocrine L cells. Nat. Commun. *6*, 7629.
25. Wang, Z., Pang, J., Wang, L., Dong, Q., and Jin, D. (2022). CEBPB regulates the bile acid receptor FXR to accelerate colon cancer progression by modulating aerobic glycolysis. J. Clin. Lab. Anal. *36*, e24703.
26. Vaquero, J., Briz, O., Herraez, E., Muntané, J., and Marin, J.J.G. (2013). Activation of the nuclear receptor FXR enhances hepatocyte chemoprotection and liver tumor chemoresistance against genotoxic compounds. Biochim. Biophys. Acta *1833*, 2212–2219.
27. Zhang, L., Wang, Y.D., Chen, W.D., Wang, X., Lou, G., Liu, N., Lin, M., Forman, B.M., and Huang, W. (2012). Promotion of liver regeneration/repair by farnesoid X receptor in both liver and intestine in mice. Hepatology *56*, 2336–2343.
28. Domínguez-Andrés, J., Dos Santos, J.C., Bekkering, S., Mulder, W.J.M., van der Meer, J.W.M., Riksen, N.P., Joosten, L.A.B., and Netea, M.G. (2023). Trained immunity: adaptation within innate immune mechanisms. Physiol. Rev. *103*, 313–346.
29. De Bont, R., and van Larebeke, N. (2004). Endogenous DNA damage in humans: a review of quantitative data. Mutagenesis *19*, 169–185.
30. Glassner, B.J., Weeda, G., Allan, J.M., Broekhof, J.L., Carls, N.H., Donker, I., Engelward, B.P., Hampson, R.J., Hersmus, R., Hickman, M.J., et al. (1999). DNA repair methyltransferase (Mgmt) knockout mice are sensitive to the lethal effects of chemotherapeutic alkylating agents. Mutagenesis *14*, 339–347.
31. Erasimus, H., Gobin, M., Niclou, S., and Van Dyck, E. (2016). DNA repair mechanisms and their clinical impact in glioblastoma. Mutat. Res. Rev. Mutat. Res. *769*, 19–35.
32. Weiler, M., Blaes, J., Pusch, S., Sahm, F., Czabanka, M., Luger, S., Bunse, L., Solecki, G., Eichwald, V., Jugold, M., et al. (2014). mTOR target NDRG1 confers MGMT-dependent resistance to alkylating chemotherapy. Proc. Natl. Acad. Sci. USA *111*, 409–414.
33. Li, W., Moorlag, S.J.C.F.M., Koeken, V.A.C.M., Röring, R.J., de Bree, L.C.J., Mourits, V.P., Gupta, M.K., Zhang, B., Fu, J., Zhang, Z., et al. (2023). A single-cell view on host immune transcriptional response to in vivo BCG-induced trained immunity. Cell Rep. *42*, 112487.
34. Kalafati, L., Kourtzelis, I., Schulte-Schrepping, J., Li, X., Hatzioannou, A., Grinenko, T., Hagag, E., Sinha, A., Has, C., Dietz, S., et al. (2020). Innate Immune Training of Granulopoiesis Promotes Anti-tumor Activity. Cell *183*, 771–785.e12.
35. Shi, J., Hua, L., Harmer, D., Li, P., and Ren, G. (2018). Cre Driver Mice Targeting Macrophages. Methods Mol. Biol. *1784*, 263–275.
36. Ross, F.A., MacKintosh, C., and Hardie, D.G. (2016). AMP-activated protein kinase: a cellular energy sensor that comes in 12 flavours. FEBS J. *283*, 2987–3001.
37. Keerthana, C.K., Rayginia, T.P., Shifana, S.C., Anto, N.P., Kalimuthu, K., Isakov, N., and Anto, R.J. (2023). The role of AMPK in cancer metabolism and its impact on the immunomodulation of the tumor microenvironment. Front. Immunol. *14*, 1114582.
38. Chen, X., Li, X., Zhang, W., He, J., Xu, B., Lei, B., Wang, Z., Cates, C., Rousselle, T., and Li, J. (2018). Activation of AMPK inhibits inflammatory response during hypoxia and reoxygenation through modulating JNK-mediated NF-kappaB pathway. Metabolism *83*, 256–270.
39. Hu, M., Ye, P., Liao, H., Chen, M., and Yang, F. (2016). Metformin Protects H9C2 Cardiomyocytes from High-Glucose and Hypoxia/Reoxygenation Injury via Inhibition of Reactive Oxygen Species Generation and Inflammatory Responses: Role of AMPK and JNK. J. Diabetes Res. *2016*, 2961954.
40. Mancini, S.J., and Salt, I.P. (2018). Investigating the Role of AMPK in Inflammation. Methods Mol. Biol. *1732*, 307–319.
41. Nassif, R.M., Chalhoub, E., Chedid, P., Hurtado-Nedelec, M., Raya, E., Dang, P.M.C., Marie, J.C., and El-Benna, J. (2022). Metformin Inhibits ROS Production by Human M2 Macrophages via the Activation of AMPK. Biomedicines *10*, 319.
42. Arts, R.J.W., Carvalho, A., La Rocca, C., Palma, C., Rodrigues, F., Silvestre, R., Kleinnijenhuis, J., Lachmandas, E., Gonçalves, L.G., Belinha, A., et al. (2016). Immunometabolic Pathways in BCG-Induced Trained Immunity. Cell Rep. *17*, 2562–2571.
43. Liu, L., Dai, X., Yin, S., Liu, P., Hill, E.G., Wei, W., and Gan, W. (2022). DNA-PK promotes activation of the survival kinase AKT in response to DNA damage through an mTORC2-ECT2 pathway. Sci. Signal. *15*, eabh2290.
44. Sobanski, T., Rose, M., Suraweera, A., O'Byrne, K., Richard, D.J., and Bolderson, E. (2021). Cell Metabolism and DNA Repair Pathways: Implications for Cancer Therapy. Front. Cell Dev. Biol. *9*, 633305.
45. Garcia, D., and Shaw, R.J. (2017). AMPK: Mechanisms of Cellular Energy Sensing and Restoration of Metabolic Balance. Mol. Cell *66*, 789–800.
46. Bertolini, A., Fiorotto, R., and Strazzabosco, M. (2022). Bile acids and their receptors: modulators and therapeutic targets in liver inflammation. Semin. Immunopathol. *44*, 547–564.
47. Fiorucci, S., Baldoni, M., Ricci, P., Zampella, A., Distrutti, E., and Biagioli, M. (2020). Bile acid-activated receptors and the regulation of macrophages function in metabolic disorders. Curr. Opin. Pharmacol. *53*, 45–54.
48. Fiorucci, S., Antonelli, E., Rizzo, G., Renga, B., Mencarelli, A., Riccardi, L., Orlandi, S., Pellicciari, R., and Morelli, A. (2004). The nuclear receptor SHP mediates inhibition of hepatic stellate cells by FXR and protects against liver fibrosis. Gastroenterology *127*, 1497–1512.
49. Fiorucci, S., Biagioli, M., Zampella, A., and Distrutti, E. (2018). Bile Acids Activated Receptors Regulate Innate Immunity. Front. Immunol. *9*, 1853.
50. Mencarelli, A., Renga, B., Migliorati, M., Cipriani, S., Distrutti, E., Santucci, L., and Fiorucci, S. (2009). The bile acid sensor farnesoid X receptor is a modulator of liver immunity in a rodent model of acute hepatitis. J. Immunol. *183*, 6657–6666.
51. Vavassori, P., Mencarelli, A., Renga, B., Distrutti, E., and Fiorucci, S. (2009). The bile acid receptor FXR is a modulator of intestinal innate immunity. J. Immunol. *183*, 6251–6261.
52. Carling, D. (2017). AMPK signalling in health and disease. Curr. Opin. Cell Biol. *45*, 31–37.
53. Li, R., Luo, X., Zhu, Y., Zhao, L., Li, L., Peng, Q., Ma, M., and Gao, Y. (2017). ATM signals to AMPK to promote autophagy and positively regulate DNA damage in response to cadmium-induced ROS in mouse spermatocytes. Environ. Pollut. *231*, 1560–1568.
54. Tripathi, D.N., Chowdhury, R., Trudel, L.J., Tee, A.R., Slack, R.S., Walker, C.L., and Wogan, G.N. (2013). Reactive nitrogen species regulate autophagy through ATM-AMPK-TSC2-mediated suppression of

mTORC1. Proc. Natl. Acad. Sci. USA *110*, E2950–E2957.
55. Szewczuk, M., Boguszewska, K., Kaźmierczak-Barańska, J., and Karwowski, B.T. (2020). The role of AMPK in metabolism and its influence on DNA damage repair. Mol. Biol. Rep. *47*, 9075–9086.
56. Wu, C.L., Qiang, L., Han, W., Ming, M., Viollet, B., and He, Y.Y. (2013). Role of AMPK in UVB-induced DNA damage repair and growth control. Oncogene *32*, 2682–2689.
57. He, P., Li, Z., Xu, F., Ru, G., Huang, Y., Lin, E., and Peng, S. (2020). AMPK Activity Contributes to G2 Arrest and DNA Damage Decrease via p53/p21 Pathways in Oxidatively Damaged Mouse Zygotes. Front. Cell Dev. Biol. *8*, 539485.
58. Zhou, Z., Luo, G., Li, C., Zhang, P., Chen, W., Li, X., Tang, J., and Qing, L. (2023). Metformin induces M2 polarization via AMPK/PGC-1alpha/PPAR-gamma pathway to improve peripheral nerve regeneration. Am. J. Transl. Res. *15*, 3778–3792.
59. Niture, S.K., Doneanu, C.E., Velu, C.S., Bailey, N.I., and Srivenugopal, K.S. (2005). Proteomic analysis of human O6-methylguanine-DNA methyltransferase by affinity chromatography and tandem mass spectrometry. Biochem. Biophys. Res. Commun. *337*, 1176–1184.
60. Duan, Z., Person, R.E., Lee, H.H., Huang, S., Donadieu, J., Badolato, R., Grimes, H.L., Papayannopoulou, T., and Horwitz, M.S. (2007). Epigenetic regulation of protein-coding and microRNA genes by the Gfi1-interacting tumor suppressor PRDM5. Mol. Cell Biol. *27*, 6889–6902.
61. Porter, L.F., Galli, G.G., Williamson, S., Selley, J., Knight, D., Elcioglu, N., Aydin, A., Elcioglu, M., Venselaar, H., Lund, A.H., et al. (2015). A role for repressive complexes and H3K9 di-methylation in PRDM5-associated brittle cornea syndrome. Hum. Mol. Genet. *24*, 6565–6579.
62. Viceconte, N., Burguillos, M.A., Herrera, A.J., De Pablos, R.M., Joseph, B., and Venero, J.L. (2015). Neuromelanin activates proinflammatory microglia through a caspase-8-dependent mechanism. J. Neuroinflammation *12*, 5.
63. Lai, C.F., Lin, S.L., Chiang, W.C., Chen, Y.M., Wu, V.C., Young, G.H., Ko, W.J., Kuo, M.L., Tsai, T.J., and Wu, K.D. (2014). Blockade of cysteine-rich protein 61 attenuates renal inflammation and fibrosis after ischemic kidney injury. Am. J. Physiol. Renal Physiol. *307*, F581–F592.
64. Minashima, T., Campbell, K.A., Hadley, S.R., Zhang, Y., and Kirsch, T. (2014). The role of ANK interactions with MYBBP1a and SPHK1 in catabolic events of articular chondrocytes. Osteoarthritis Cartilage *22*, 852–861.
65. Wongchana, W., Lawlor, R.G., Osborne, B.A., and Palaga, T. (2015). Impact of Notch1 Deletion in Macrophages on Proinflammatory Cytokine Production and the Outcome of Experimental Autoimmune Encephalomyelitis. J. Immunol. *195*, 5337–5346.
66. Kim, D., Paggi, J.M., Park, C., Bennett, C., and Salzberg, S.L. (2019). Graph-based genome alignment and genotyping with HISAT2 and HISAT-genotype. Nat. Biotechnol. *37*, 907–915.
67. Liao, Y., Smyth, G.K., and Shi, W. (2014). featureCounts: an efficient general purpose program for assigning sequence reads to genomic features. Bioinformatics *30*, 923–930.
68. Liao, Y., Smyth, G.K., and Shi, W. (2013). The Subread aligner: fast, accurate and scalable read mapping by seed-and-vote. Nucleic Acids Res. *41*, e108.
69. Love, M.I., Huber, W., and Anders, S. (2014). Moderated estimation of fold change and dispersion for RNA-seq data with DESeq2. Genome Biol. *15*, 550.
70. Subramanian, A., Tamayo, P., Mootha, V.K., Mukherjee, S., Ebert, B.L., Gillette, M.A., Paulovich, A., Pomeroy, S.L., Golub, T.R., Lander, E.S., and Mesirov, J.P. (2005). Gene set enrichment analysis: a knowledge-based approach for interpreting genome-wide expression profiles. Proc. Natl. Acad. Sci. USA *102*, 15545–15550.
71. Liberzon, A., Subramanian, A., Pinchback, R., Thorvaldsdóttir, H., Tamayo, P., and Mesirov, J.P. (2011). Molecular signatures database (MSigDB) 3.0. Bioinformatics *27*, 1739–1740.
72. Liberzon, A., Birger, C., Thorvaldsdóttir, H., Ghandi, M., Mesirov, J.P., and Tamayo, P. (2015). The Molecular Signatures Database (MSigDB) hallmark gene set collection. Cell Syst. *1*, 417–425.
73. Martens, M., Ammar, A., Riutta, A., Waagmeester, A., Slenter, D.N., Hanspers, K., A Miller, R., Digles, D., Lopes, E.N., Ehrhart, F., et al. (2021). WikiPathways: connecting communities. Nucleic Acids Res. *49*, D613–D621.
74. Walachowski, S., Tabouret, G., Fabre, M., and Foucras, G. (2017). Molecular Analysis of a Short-term Model of beta-Glucans-Trained Immunity Highlights the Accessory Contribution of GM-CSF in Priming Mouse Macrophages Response. Front. Immunol. *8*, 1089.
75. Malone, H.E., Nicholl, H., and Coyne, I. (2016). Fundamentals of estimating sample size. Nurse Res. *23*, 21–25.
76. Keating, S.T., Groh, L., van der Heijden, C.D.C.C., Rodriguez, H., Dos Santos, J.C., Fanucchi, S., Okabe, J., Kaipananickal, H., van Puffelen, J.H., Helder, L., et al. (2020). The Set7 Lysine Methyltransferase Regulates Plasticity in Oxidative Phosphorylation Necessary for Trained Immunity Induced by beta-Glucan. Cell Rep. *31*, 107548.
77. Livak, K.J., and Schmittgen, T.D. (2001). Analysis of relative gene expression data using real-time quantitative PCR and the 2(-Delta Delta C(T)) Method. Methods *25*, 402–408.

STAR★METHODS

KEY RESOURCES TABLE

REAGENT or RESOURCE	SOURCE	IDENTIFIER
Antibodies		
Rat monoclonal anti-mouse F4/80	BioLegend	Cat# 123120; RRID: AB_893479
Rat monoclonal anti-mouse/human CD11b	BioLegend	Cat# 101208; RRID: AB_312791
Rat monoclonal anti-mouse MGMT	R&D Systems	Cat# 300008; RRID: AB_2143208
Rabbit monoclonal anti-phospho AKT (Thr308)	Cell Signaling Technology	Cat# 2965; RRID: AB_2255933
Rabbit polyclonal anti-AKT	Cell Signaling Technology	Cat# 9272; RRID: AB_329827
Rabbit monoclonal anti-phospho NF-κB p65	Cell Signaling Technology	Cat# 3033; RRID: AB_331284
Rabbit polyclonal anti-NF-κB p65	Cell Signaling Technology	Cat# 3987; RRID: AB_2341215)
Rabbit monoclonal anti-phospho ERK1/2	Cell Signaling Technology	Cat# 4370; RRID: AB_2315112
Rabbit monoclonal anti-ERK1/2	Cell Signaling Technology	Cat# 4695; RRID: AB_390779
Rabbit monoclonal anti-phospho p38	Cell Signaling Technology	Cat# 4511; RRID: AB_2139682
Rabbit monoclonal anti-p38	Cell Signaling Technology	Cat# 8690; RRID: AB_10999090
Rabbit monoclonal anti-phospho SAPK/JNK	Cell Signaling Technology	Cat# 4668; RRID: AB_823588
Rabbit monoclonal anti-SAPK/JNK	Cell Signaling Technology	Cat# 9252; RRID: AB_2250373
Rabbit polyclonal anti-phospho mTOR (Ser2448)	Cell Signaling Technology	Cat# 2971; RRID: AB_330970
Rabbit polyclonal anti-mTOR	Cell Signaling Technology	Cat# 2972; RRID: AB_330978
Rabbit monoclonal anti-HIF1α	Cell Signaling Technology	Cat# 36169; RRID: AB_2799095
Rabbit monoclonal anti-phospho AMPK alpha (Thr172)	Cell Signaling Technology	Cat# 2535; RRID: AB_331250
Rabbit monoclonal anti-AMPK alpha	Cell Signaling Technology	Cat# 5832; RRID: AB_10624867
Mouse monoclonal anti-β-actin	Cell Signaling Technology	Cat# 3700; RRID: AB_2242334
Rabbit polyclonal anti-GAPDH	Bio-Rad	Cat# AHP1628; RRID: AB_1604986
Mouse monoclonal anti-ATM phospho (Ser1981)	BioLegend	Cat# 651202; RRID: AB_10900251
Rabbit monoclonal anti-phospho H2A.X	Cell Signaling Technology	Cat# 9718; RRID: AB_2118009
Goat anti-rat IgG, HRP-linked Antibody	BioLegend	Cat# 405405; RRID: AB_315016
Goat anti-rabbit IgG, HRP-linked Antibody	Cell Signaling Technology	Cat# 7074; RRID: AB_2099233
Sheep anti-mouse IgG, HRP-linked Antibody	Cytiva	Cat# NA9310-1mL; RRID: AB_772193
Anti-rabbit IgG, Alexa Fluor® 488 Conjugate	Cell Signaling Technology	Cat# 4412; RRID: AB_1904025
Anti-mouse IgG, Alexa Fluor® 555 Conjugate	Cell Signaling Technology	Cat# 4409; RRID: AB_1904022
Purified anti-mouse IL-6 Antibody	BioLegend	Cat# 504502; RRID: AB_315336
Biotin anti-mouse IL-6 Antibody	BioLegend	Cat# 504601; RRID: AB_2127458
Chemicals, peptides, and recombinant proteins		
Lomeguatrib	Sellekchem	Cat#S8056
Ursodeoxycholic acid (UDCA)	Sellekchem	Cat#S1643
Pachyman (1,3-β-D-Glucan)	Megazyme	CAS: 9037-88-1
Lipopolysaccharides from *Escherichia coli*	Sigma-Aldrich	Cat#l2880
Normal Goat Serum	Cell Signaling Technology	Cat#5425
Hoechst 3342	Thermo Fisher Scientific	Cat#H3570
Lipofectamine 2000	Thermo Fisher Scientific	Cat#11668027
Critical commercial assays		
ELISA MAX™ Standard Set Mouse TNF-α	BioLegend	Cat#430901
LEGENDplex™ Mouse Inflammation Panel (13-plex) with V-bottom Plate	BioLegend	Cat#740446

(*Continued on next page*)

Continued

REAGENT or RESOURCE	SOURCE	IDENTIFIER
Pierce™ BCA Protein Assay Kits	Thermo Fisher Scientific	Cat#23225
Seahorse XF Glycolysis Stress Test Kit	Agilent Technologies	Cat#103020-100
Deposited data		
Raw and analyzed data (DEGs list)	This paper	GEO: GSE231419
Raw Western blot data (deposited on Mendeley)	This paper	https://doi.org/10.17632/f3bfnwgddv.1
Experimental models: Cell lines		
NCTC clone 929 (L-929 cell line)	ATCC	Cat# CCL-1; RRID: CVCL_0462
Experimental models: Organisms/strains		
C57BL/6 mice	Nomura Siam International	N/A
LysM-cre$^{cre/+}$; MGMT$^{fl/fl}$ mice (MGMT KO)	Cyagen Biosciences (Suzhou) Inc.	N/A
LysM-cre$^{+/+}$; MGMT$^{fl/fl}$ mice	Cyagen Biosciences (Suzhou) Inc.	N/A
Oligonucleotides		
Accell™ SMARTpool siRNA targeted murine *Mgmt*	Horizon Discovery	Cat# E−047426-00-0005
Accell™ non-targeting control pool	Horizon Discovery	Cat# D-001910-10-05
Primer: *Mgmt* F: 5′-GCTCTCCATCACCCTGTGTT-3′ and R: 5′-ATGAGGATGGG GACCGGATTG-3′;	This paper	N/A
Primer: *Tnf* F: 5′-AGCCCACGTCGTAGCAAACCAC-3′ and R: 5′-ATCGGCTGGCACCACTAGTTGGT-3′	Viceconte, N. et al.[62]	N/A
Primer: *Il1b* F: 5′-TATACCTGTCCTGTG TAA-3 and R: 5′-TTGACTTCTATCTTGTTGA-3′	Lai, C.F. et al.[63]	N/A
Primer: *Il6* F: 5′-CTCTGGGAAATCGTGGAA ATG-3′ and R: 5′-AAGTGCATCATCGTTGTTCATACA-3′	Minashima, T. et al.[64]	N/A
Primer: *Actn* F: 5′-ACCAACTGGGACGACATGGAGAA-3′ and R: 5′ GTGGTGGTGAAGCTGTAGCC-3′	Wongchana, W. et al.[65]	N/A
Software and algorithms		
LEGENDplex™ Data Analysis Software	BioLegend	https://www.biolegend.com/ja-jp/legendplex#software
ImageJ	National Institutes of Health	RRID:SCR_003070
Hisat2	Kim, D et al.[66]	RRID:SCR_015530
Agilent Seahorse Wave	Agilent Technologies	RRID:SCR_024491
R package Rsubread, featureCounts	Liao, Y et al.[67,68]	RRID:SCR_016945
R package DESeq2	Love, M. I. et al.[69]	RRID:SCR_015687
R package pheatmap	https://cran.r-project.org/web/packages/pheatmap/index.html	RRID:SCR_016418
Venn Diagram	https://bioinformatics.psb.ugent.be/webtools/Venn/	N/A
GSEA version 4.3.2	Subramanian, A. et al.[70]	RRID:SCR_003199
Molecular Signatures Database (MSigDB)	Liberzon, A.[71,72]	RRID:SCR_016863
Wikipathways version 2022.1	Martens M et al.[73]	RRID:SCR_002134
GraphPad Prism version 9.0	GraphPad Prism	RRID:SCR_002798
ZEISS ZEN 3.5 (blue edition)	Zeiss	N/A

(*Continued on next page*)

Continued

REAGENT or RESOURCE	SOURCE	IDENTIFIER
Other		
RNeasy® Mini Kit	Qiagen	N/A
iQ™ SYBR Green Supermix	Bio-Rad	N/A

RESOURCE AVAILABILITY

Lead contact

Further information and requests for resources and reagents should be directed to and will be fulfilled by the lead contact, Tanapat Palaga (tanapat.p@chula.ac.th).

Materials availability

This study did not generate new unique reagents.

Data and code availability

- All data reported in this paper will be shared by the lead contact upon request.
- RNA-seq data have been deposited at GEO and are publicly available as of the date of publication. Accession numbers are listed in the key resources table.
- Original western blot images have been deposited at Mendeley and are publicly available as of the date of publication. The DOI is listed in the key resources table.
- Microscopy data reported in this paper will be shared by the lead contact upon request.
- This paper does not report original code.
- Any additional information required to reanalyze the data reported in this paper is available from the lead contact upon request.

EXPERIMENTAL MODEL AND STUDY PARTICIPANT DETAILS

Construction of mouse model

Mice with specific knock out of *Mgmt* in myeloid cells (MGMT KO, LysM-cre$^{cre/+}$; MGMT$^{fl/fl}$) was generated by the Cre/*loxP* system. To generate the MGMT-loxP strain (MGMT$^{fl/fl}$), the *loxP* sequence was inserted into exon 3 of *Mgmt* gene in the fertilized mouse eggs of C57BL/6 mice by CRISPR/cas9 system (Cyagen Biosciences (Suzhou) Inc., Jiangsu, China). The MGMT floxed strain was bred with the LysM-Cre strain (LysM-cre$^{cre/+}$, Cyagen Biosciences (Suzhou) Inc., Jiangsu, China) to generate the MGMT KO mice. The littermate control mice (LysM-cre$^{+/+}$; MGMT$^{fl/fl}$) from the same litter were used as control. All animals were housed under specific pathogen free conditions at Chulalongkorn University Laboratory Animal Center, Bangkok, Thailand (approval protocol No. 2073016). All experiments were performed according to the guidelines issued by the IACUC.

Isolation and culture of bone marrow derived macrophages (BMMs)

Eight-to-ten-week-old C57BL/6 mice (both sex) purchased from Nomura Siam International (Thailand) were used as a source of bone marrow cells in some experiments. For generation of BMMs, bone marrow cells extracted from the tibia and femur of MGMT KO mice or littermate control (WT BMMs). For bone marrow differentiation, the bone marrow cells were cultured in Dulbecco's modified Eagle's medium (DMEM) (HyClone, USA) supplemented with 10% (v/v) fetal bovine serum (Gibco, USA), 10 mM HEPES (HyClone), 1 mM sodium pyruvate (HyClone), 100 U/mL penicillin, and 0.25 mg/mL streptomycin (DMEM complete media) with 20% L929 culture supernatant and 5% horse serum (HyClone, USA), and fresh media was added at day 4. After 7 days in culture, cells were harvested with cold PBS and stored at −80°C until use. Differentiation of BMMs were confirmed by flow cytometry using macrophage specific surface markers, F4/80 and CD11b. Experimental procedures involving laboratory animals were approved by the Institutional Animal Care and Use Committee (IACUC) of the Faculty of Medicine, Chulalongkorn University, Bangkok, Thailand (approval protocol No. 025/2562) and Chulalongkorn University Laboratory Animal Center, Bangkok, Thailand (approval protocol No. 2073016). All experiments were performed according to the guidelines issued by the IACUC.

METHOD DETAILS

Generation of BG-trained BMMs

BMMs were cultured in complete DMEM and primed with pachyman BG (50 μg/mL; Megazyme, USA). After 24 h of priming, the medium was replaced with fresh DMEM complete medium, and and the cells were rested for 48 h.[16,74] The resting step was followed by stimulation with *Escherichia coli* LPS (10 ng/mL; L2880, Sigma Aldrich, USA) for the indicated times. Culture supernatant, total RNA or cell lysates were harvested at the indicated times for analysis. The amount of TNFα and IL-6 in the culture supernatant was measured by mouse TNFα and IL-6 ELISA (Biolegend, USA) according to the manufacturer's protocol.

For inhibitor treatment, the MGMT inhibitor lomeguatrib or the FXR inhibitor ursodeoxycholic acid (UDCA) (both were from Selleckhem, USA) was added at indicated time points. The amount of cytokines was measured by ELISA as described above and compared with the vehicle control treatment.

siRNA mediated silencing of *Mgmt* expression

AccellSMARTpool siRNA targeted murine *Mgmt* (Horizon Discovery, UK) and the transfection reagent Lipofectamine 2000 (Promega, Wisconsin, USA) were prepared in Opti-MEMI Reducing-Serum Media (Gibco, USA). After incubation of siRNA/transfection reagent, the lipid-siRNA complex in Opti-MEM was applied to unstimulated BMMs. The final concentration of siRNA and Lipofectamine are 50 nM and 0.6%. Following the incubation for 6 h, transfection media were replaced with fresh BMM media. The reduction in *Mgmt* mRNA and protein was confirmed at 48 h after siRNA transfection by qRT-PCR and Western blot as described above. The trained immunity was induced by BG treatment in *Mgmt* silencing macrophages as described above. The amount of TNFα and IL-6 in the culture supernatant at 24 h after LPS stimulation was measured by ELISA. The BMMs transfected with Accellnon-targeting control pool (Horizon Discovery, UK) were used as control.[16]

In vivo model for trained immunity

Trained immunity in eight to ten weeks old MGMT KO and littermate control mice (either sex, n = 4–6 mice per group) were induced by intraperitoneal injection with pachyman BG (1 mg per animal) and PBS was used as control. As we focused and compared the levels of cytokines between WT vs. MGMT KO after BG/LPS injection, the sample size was estimated using sample size calculation for two independent group with expected success rate to be 0.95 (β = 0.05) and the false positive rate between 0.1 and 0.01 (α = 0.1–0.01).[75] After 5 days, all mice were intraperitoneal injected with *E. coli* LPS (10 μg per animal) with PBS as control.[76] Blood cytokines were detected at 3 h after LPS injection by LEGENDplex Mouse Inflammation Panel (Biolegend, USA) following the company's instruction. Levels of cytokine production were measured by flow cytometry. Data were analyzed using The LEGENDplex Data Analysis Software Suite (https://www.biolegend.com/ja-jp/legendplex#software).

Complete blood count assay

Whole blood from eight-to-ten-week-old WT and MGMT KO mice were collected from submandibular facial vein. Fifty to hundred μL of whole blood in EDTA tube were subjected to a complete blood count assay using VETSCAN HM5 Hematology Analyzer (Zoetis Inc., USA) at Central Animal Facility, Faculty of Science, Mahidol University, Bangkok, Thailand.

RNA sequencing and data analysis

Unstimulated, BG-primed (BG24) and BG-primed with LPS stimulation (BG/LPS) BMMs were prepared as described above. Total RNA from each sample were extracted using RNeasy Mini Kit (Qiagen, USA) following the manufacturer's protocol. 0.5–1 mg of total RNAs were subjected to RNA quality assessment using the 2100 Bioanalyzer (Agilent Technology, USA). All RNA samples in this study acquired RNA integrity number (RIN) scores greater than 7.0 and 28S/18S ratio greater than 1. RNA sequencing was carried out using a DNBSEQ sequencing technology at BGI sequencing center, Hong Kong (paired end read with 150 bp/read).

RNA-Seq analysis Sequencing reads were mapped against the *Mus musculus* reference genome GRCm39. Reads were mapped and aligned with Hisat2[66] and counted using the R package Rsubread, featureCounts.[67,68] Then, differential expressed genes (DEGs) were compared and analyzed using the R package DESeq2 with the p value cut off < 0.05.[69] To focus on the effect of MGMT KO in trained immunity, the normalized counts of DEGs in BG24 and BG/LPS were normalized to the normalized counts unstimulated WT BMMs. The heatmap of DEGs in BG24 and BG/LPS were created using the R package pheatmap. Lists of up- or down-regulated DEGs in each condition were compared using Venn Diagram (https://bioinformatics.psb.ugent.be/webtools/Venn/). DEGs that specifically upregulated in each condition were subjected to perform Gene Set Enrichment Analysis (GSEA) using GSEA version 4.3.2.[70] DEGs and its log2FoldChange from DESeq2 were used as input for GSEA pre-rank analysis. Mouse Gene Symbol Remapping Human Orthologs MSigDB version 2022.1.HS was selected as chip platform.[71,72] Wikipathway version 2022.1 was selected as searching database.[73] Significant GSEA pathway were selected with p value <0.05 and FDR <0.25. DEGs that are associated with a DNA damage and DNA repair mechanism were manually filtered from up-regulated DEGs in MGMT KO BMMs (BG24 and BGLPS) based on literature search (see Table S1). The datasets generated or analyzed for this study were deposited in a public database and can be found under the GEO: GSE231419.

Western blot

BMMs were treated as described above. Cell lysates were collected at the indicated times using RIPA buffer (50 mM Tris HCl pH 7.4, 150 mM (for MGMT and TLR4 signaling proteins) or 500 mM (for other proteins) NaCl, 5 mM EDTA, 1% nonidet P-40, 0.5% sodium deoxycholate supplemented with protease and phosphate inhibitors (Cell Signaling Technology, USA)). The protein concentrations were measured by a bicinchoninic acid assay using the Pierce BCA Protein Assay Kit (Thermo-Fisher Scientific, USA). Proteins were resolved by 8% (for AKT, mTOR, HIF1α, and TLR4 signaling proteins) and 15% (for MGMT) SDS-PAGE and subjected to Western blot as described elsewhere. All antibodies used in this study were purchased from R&D (for MGMT) and Cell Signaling Technology (for other proteins). The antibodies were diluted in the buffer according to the the manufacturer's protocol at the following concentration: rat anti-mMGMT, 1:2000 (R&D Systems, USA); rabbit anti-phospho AKT (Thr308), 1:1000; rabbit anti-AKT, 1:1000; rabbit anti-phospho NF-κB p65, 1:2000; rabbit anti-NF-κB p65, 1:4000; rabbit

anti-phospho ERK1/2, 1:2000; rabbit anti-ERK1/2, 1:4000; rabbit anti-phospho p38, 1:2000; rabbit anti-p38, 1:4000; rabbit anti-phospho SAPK-JNK, 1:2000; rabbit anti-SAPK-JNK, 1:4000; rabbit anti-phospho mTOR, 1:1000; rabbit anti-mTOR, 1:1000; rabbit anti-HIF1α, rabbit anti-phospho AMPK alpha, 1:2000; rabbit anti-AMPK alpha, 1:2000; anti-actin antibody, 1:10000; and goat anti-rabbit IgG HRP, 1:4000 (all antibodies were purchased from Cell Signaling Technology, USA); goat anti-rat IgG HRP, 1:4000 (Biolegend, USA); sheep anti-mouse IgG HRP, 1:4000 (Cytiva, USA); rabbit polyclonal anti-GAPDH, 1:4000 (Bio-Rad, USA).The signal was detected by the ECL chemiluminescent detection method. Relative intensity was analyzed by ImageJ analysis. Raw Western blot data from all figures were deposited on Mendeley data: https://doi.org/10.17632/f3bfnwgddv.1.

RT-qPCR

BMMs were treated as indicated in each experiment. Total RNA was harvested and extracted with RNeasy Mini Kit (Qiagen, USA). The quality and concentrations of RNA were measured by a NanoDrop 2000 spectrophotometer (Thermo Fisher Scientific, USA). Two hundred nanograms of RNA per sample was converted to cDNA, which was used for quantitative PCR using iQ SYBR Green SuperMix (Bio-Rad, USA) according to the manufacturer's instructions. The primers used in this study are shown as follow: *Mgmt* F: 5′-GCTCTCCATCACCCTGTGTT-3′ and R: 5′-ATGAGGATGGG GACCGGATTG-3′; *Tnf* F: 5′-AGCCCACGTCGTAGCAAACCAC-3′ and R: 5′-ATCGGCTGGCACCACTAGTTG GT-3′[62]; *Il1b* F: 5′-TATACCTGTCCTGTG TAA-3 and R: 5′-TTGACTTCTATCTTGTTGA-3′[63]; *Il6* F: 5′-CTCTGGGAAATCGTGGAA ATG-3′ and R: 5′-AAGTGCATCATCGTTGTTCATACA-3′[64]; *Actn* F: 5′-ACCAACTG GGACGACATGGAGAAA-3′ and R: 5′-GTGGTGGTGAAGCTG TAGCC-3′.[65] The relative expression of all target genes was normalized to the expression of *Actb* by the $2^{-\Delta\Delta CT}$ method and calculated by comparison with that of ctrl LPS or unstimulated cells.[77]

MTT assay

BMMs were treated with inhibitors as indicated in each experiment. After 20 h of LPS stimulation, MTT reagent was added to a final concentration of 0.5 mg/mL. After incubation with MTT reagent for 4 h, 200 μL of DMSO was added to each well to dissolve the MTT formazan pellet. The intensity of the pellet was measured by a microplate reader at a wavelength of 540 nm.

Immunofluorescence staining of DNA damage and DNA repair markers

WT and MGMT KO BMMs were cultured at 4×10^5 cells/well in 4-well chamber slides (Thermo Fisher Scientific). Trained immunity was induced as indicated in Figure 1A. BMMs were fixed with 4% paraformaldehyde (Sigma-Aldrich, USA) after BG treatment and LPS restimulation. Samples were blocked and permeabilized with 5% normal goat serum (Cell Signaling Technology, USA) and 0.3% Triton X-100 (Amersham Biosciences, Little Chalfont, UK) in PBS buffer. The antibodies against mouse anti-phosphor-ATM (Biolegend, USA) and rabbit anti-γH2AX (Cell Signaling Technology, USA) were diluted in 1% bovine serum albumin (Sigma-Aldrich, USA), 0.3% Triton X-100 in PBS buffer at 1:500. After incubation overnight, fluorescent dye-conjugated secondary antibodies, including anti-rabbit IgG antibody conjugated with Alexa Fluor 488 and anti-mouse IgG antibody conjugated with Alexa Fluor 555 (both from Cell Signaling Technology, USA), were used for detection. Nuclei were stained with Hoechst 3342 (Thermo Fisher Scientific, USA). Images were acquired with a Confocal microscope LSM 980 with Airyscan 2 (Carl Zeiss AG, Germany) and prepared by ZEISS ZEN 3.5 (blue edition, Carl Zeiss AG, Germany). Mean fluorescence intensity (MFI) in each condition was measured from at least 90 positive cells by ImageJ analysis.

Glycolysis stress assay

Approximately 1×10^5 cells of BMMs were plated in XFp Cell Culture Miniplate (Agilent Technologies, USA) overnight in BMMs media. The media were replaced with fresh DMEM complete medium and the cells were rested for 1 h before stimulation with BG (50 μg/mL) for 24 h. After resting for 48 h, glycolytic function was detected using Agilent Seahorse XF Glycolysis Stress Test Kit (Agilent Technologies, USA) following the manufacturer's protocol. The glycolysis signal was measured by extracellular acidification rate (ECAR) by Agilent Seahorse XFp Analyzer (Agilent Technologies, USA). In brief, BMMs were incubated in glucose free assay medium and non-glycolysis acidification was measured. This step was followed by addition of glucose to the system (final concentration = 10 mM) to induce glycolysis function. Oligomycin, an ATP synthase inhibitor (final concentration = 50 mM) was added to inhibit the mitochondria function leading to induce the maximum glycolysis. Finally, 2-DG, a glycolysis inhibitor (final concentration = 500 mM) was added to confirm that ECAR signal in this system represents the glycolytic function. The data were analyzed using Agilent Seahorse Wave (Agilent Technologies, USA).

QUANTIFICATION AND STATISTICAL ANALYSIS

All experiments were performed at least in triplicate and at least twice independently. Statistical analyses were performed using GraphPad Prism version 9.0. One-way ANOVA with Dunnett's or Tukey's multiple comparison test and two-tailed unpaired (a = 0.05) were used when comparing the two conditions. All data were represented as mean ± SEM. This study is reported in accordance with ARRIVE guidelines.